

#### LIBRARY Michigan State University

This is to certify that the thesis entitled

## THE PHASE DIAGRAM OF THE DILUTED ANTIFERROMAGNET IN A FIELD AT ZERO TEMPERATURE

presented by

**Andreas Glaser** 

has been accepted towards fulfillment of the requirements for the

M.S.	_ degree in	Physics								
	Pulland									
	Major Professor's Signature									
		//								
		07/25/2003								
		Date								

MSU is an Affirmative Action/Equal Opportunity Institution

## PLACE IN RETURN BOX to remove this checkout from your record. TO AVOID FINES return on or before date due. MAY BE RECALLED with earlier due date if requested.

DATE DUE	DATE DUE	DATE DUE

6/01 c:/CIRC/DateDue.p65-p.15

# THE PHASE DIAGRAM OF THE DILUTED ANTIFERROMAGNET IN A FIELD AT ZERO TEMPERATURE

 $\mathbf{B}\mathbf{y}$ 

Andreas Glaser

#### A THESIS

Submitted to

Michigan State University
in partial fulfillment of the requirements

for the Degree of

MASTER OF SCIENCE

Department of Physics and Astronomy

2003

#### **ABSTRACT**

## THE PHASE DIAGRAM OF THE DILUTED ANTIFERROMAGNET IN A FIELD AT ZERO TEMPERATURE

By

#### Andreas Glaser

The discussion of disordered systems such as the diluted antiferromagnet in a field (DAFF) is highly controversial. Classical approaches like the renormalization group lead to contradictory results. This thesis presents alternative methods for the understanding of the low temperature regime of the DAFF. The results help to identify misunderstandings and misleading assumptions in the recent research literature.

The phase diagram of the DAFF ground state is established by a Bethe lattice mean-field theory and exact simulations of the ground state in three dimensions. By introducing an appropriate order parameter for the ground state, it is found that the DAFF exhibits three different phases. This stands in contrast to the ground state of the 3d Random Field Ising Model (RFIM) which exhibits two different phases, although the RFIM and the DAFF are supposed to be in the same universality class.

The mean-field theory phase diagram is derived by a new technique for the Bethe lattice which can also be applied to other systems. The ground state simulations are used to establish the phase diagrams for the cubic and the BCC lattice.

Für Mama und Papa

#### Acknowledgements

I would like to express my gratitude to my advisor, Phil Duxbury, for his trust, help, guidance, and many useful hints as well as his financial support. Furthermore, I would like to thank Erin McGarrity for his help with the 3d graphics and his general computer support as well as Thomas Barthel for the contribution of his program code. I also thank my thesis committee members, S.D. Mahanti and W. Pratt. Silvio Petriconi is thanked for his computer hints and many interesting off-topic discussions.

Finally, I would like to thank Wolfgang Bauer for bringing me to Michigan State University and the Studienstiftung des deutschen Volkes for the financial support and the great USA meeting in Pasadena.

### **Contents**

1	Intr	oduct	ion	1						
1.1 A brief history of disorder										
	1.2	Outline and context of the work in this thesis								
	1.3	The basics								
		1.3.1	From the crystal structure of $Fe_cZn_{1-c}F_2$ to the DAFF Hamil-							
			tonian	10						
		1.3.2	Order parameters for the DAFF	13						
2	Mea	an-field	d theory	15						
	2.1	Introd	luction to the mean-field approximations	16						
	2.2	Take I	I: A basic MFT for the DAFF	18						
		2.2.1	Neglect of the thermal fluctuations	18						
		2.2.2	Further assumptions	20						
		2.2.3	The mean-field phase diagram in the limit $z  o \infty$	23						
	2.3	Review	w of the mean-field calculations for the DAFF	28						
		2.3.1	The replica method	29						
		2.3.2	Local mean-field theory	33						
	2.4	Take I	II: A Bethe lattice MFT for the DAFF	41						
		2.4.1	The Bethe lattice	42						
		2.4.2	MFT ansatz for finite temperatures	43						

		2.4.3	An order parameter for the DAFF ground state	48
		2.4.4	A Bethe MFT for the DAFF ground state	49
	2.5	Conclu	usion	58
3	Nur	merica	l simulations of the DAFF ground state	61
	3.1	An eff	ective algorithm for the ground state calculation	61
		3.1.1	Maximum flow and minimum cut	62
		3.1.2	Mapping to maximum flow	64
		3.1.3	Transforming the bipartite DAFF into a ferromagnet	67
	3.2	Result	s of the ground state simulation	68
		3.2.1	Measurement of the order parameters	69
		3.2.2	The cubic lattice	70
		3.2.3	The BCC lattice	81
	3.3	Direct	comparison of the LMF results to the DAFF ground state	87
4	Con	clusio	n	89
Bi	bliog	graphy		92

## List of Figures

1.1	Phase diagram for the L=50 BCC lattice	7
1.2	Schematic figure of one cell of $FeF_2$	11
2.1	Phase diagram for the DAFF in the limit that the coordination number	
	z goes to infinity	28
2.2	Phase diagram from the replica calculation.	34
2.3	Phase diagram from the LMF calculation	39
2.4	Bethe lattice with z=3	42
2.5	Illustration of the bonds of site $s$ in the Cayley tree	44
2.6	Solutions of the recursion relations for $P$ and $M$	52
2.7	Solution for the recursion relations for $A$ and $B$	54
2.8	Solution of the recursion relations for $A_{\infty}$ and $B_{\infty}$	55
2.9	Solution of the recursion relations for $A_{\infty}$	56
2.10	Solution of the recursion relations for $P_{GAC}$	58
2.11	Phase diagram from the Bethe lattice MFT with $\alpha=7.$	59
3.1	Square lattice with L=400 and H=1.0J averaged over 10 samples. The	
	ordinate shows the probability that a site is in the biggest antiferro-	
	magnetic cluster (GAC1), the probability that a site is in the second	
	biggest cluster (GAC2) and the fraction of degenerate sites (deg. sites).	70
3.2	Cubic lattice with L=70 and H=3.5, one sample	71

3.3	Single samples of the cubic lattice for different lattice sizes. The ordi-	
	nate shows the probability that a site is in the biggest antiferromag-	
	netic cluster (GAC), the probability that a site is in the second biggest	
	cluster (GAC2) and the fraction of degenerate sites (degs)	73
3.4	3d plots of the cubic lattice	74
3.5	Cubic lattice with L=70 and H=3.5 averaged over 15 samples	<b>7</b> 5
3.6	Cubic lattice with L=70 and H=3.0, averaged over ten samples. The	
	ordinate shows the probability that a site is in the biggest antiferro-	
	magnetic cluster (GAC), the probability that a site is in the second	
	biggest cluster (GAC2) and the fraction of degenerate sites (degs)	76
3.7	Demonstration how to estimate the critical points	77
3.8	Cubic lattice with L=70 and H=4.1, averaged over three samples. The	
	ordinate shows the probability that a site is in the biggest ferromag-	
	netic cluster (GFC), the probability that a site is in the biggest an-	
	tiferromagnetic cluster (GAC), and the probability that a site is in	
	the second biggest antiferromagnetic cluster (GAC2), as well as the	
	fraction of degenerate sites (degs).	78
3.9	Cubic lattice with $c=0.5$ for varying values of $H.$	79
3.10	Phase diagram for the L=70 cubic lattice	80
3.11	BCC lattice with $L=50$ and $H=2.5$ , averaged over ten samples.	
	The ordinate shows the probability that a site is in the biggest antifer-	
	romagnetic cluster (GAC), the probability that a site is in the second	
	biggest cluster (GAC2) and the fraction of degenerate sites (degs)	82
3.12	BCC lattice with $L=50$ and $H=1.5$ under different boundary con-	
	ditions	83
3.13	The sublattice magnetization averaged over both sublattices for a BCC	
	lattice with $L = 50$ and $H = 2.5$ , averaged over five samples	84

3.14	BCC lattice with $L = 50$ and $H = 1.5$ under ferromagnetic boundary	
	conditions, averaged over five samples. The ordinate shows the proba-	
	bility that a site is in the biggest antiferromagnetic cluster (GAC), as	
	well as the sublattice magnetization $m_{sub}.$	84
3.15	BCC lattice with $L=50$ and $H=0.1$ under ferromagnetic boundary	
	conditions, averaged over five samples. The ordinate shows the proba-	
	bility that a site is in the biggest antiferromagnetic cluster (GAC) and	
	the probability that a site is in the second biggest cluster (GAC2)	85
3.16	Phase diagram for the L=50 BCC lattice.	86

## List of Tables

3.1	Comparison	of	the	local	me	ean-	field	the	ory	resu	ılts	to	th	e	rea	al	gr	ou	no	d	
	state																				88

### Chapter 1

#### Introduction

The understanding of the influence of disorder on critical phenomena has been one of the most challenging projects in statistical physics of the last thirty years; and it is far from being complete. The diluted antiferromagnet in a field is one of the distinguished physical systems, where the effects of disorder can be observed in action. Below we will unroll the story of how striking and contradictory results about the effects of disorder in statistical systems have led to a theoretical discussion which has been going on for decades. In this discussion the diluted antiferromagnet in a field, or DAFF, plays a central role as it describes experimental systems where the disorder can be carefully controlled.

The low temperature regime of the DAFF is the focus of this thesis. In section 1.2 it is outlined how our results for the DAFF ground state help to identify misleading assumptions and to resolve open contradictions of recent studies of disordered systems. Furthermore the results of this thesis offer a benchmark for the experiments on the DAFF.

#### 1.1 A brief history of disorder

But let us start at the beginning. The discussion of disordered systems starts with the results for thermal systems without disorder. The focus is the critical behavior of these systems and how it is influenced by disorder. As we will see below, statistical systems at the critical point exhibit very special and interesting properties. An introduction to critical phenomena and the Ising model, which is important for the further discussion can be found in [32].

Bliss for generalists: the universality principle and the renormalization group. One of the most striking experiences from the investigation of critical phenomena is the concept of universality: The critical behavior of a statistical system does not usually depend on the system's specific properties; systems can be categorized into universality classes: all systems which are within the same universality class exhibit the same critical behavior independent of the system's details. This astonishing principle which was already known from research experience in the sixties, has been demonstrated explicitly by K.G. Wilson in 1971 for the Ising model of a ferromagnet in his Nobel prize winning paper [35]. In this work Wilson has initiated a method which since then has established itself as the most powerful tool for the theoretical investigation of critical phenomena: the renormalization group. The renormalization group uses the fact that the critical behavior of a system remains invariant under variation of the relevant length scales, because the correlation length becomes infinite at the critical point. Wilson has presented a coherent way to rescale the Ising model in momentum space. The critical points are fixed points which remain invariant under this procedure. The renormalization group makes it possible to calculate all the critical exponents which completely describe the system's critical behavior. Wilson's results clarified all the universality classes of the Ising model. The exponents do not depend on an applied uniform magnetic field or the concrete

structure of the lattice but only on its dimension d. In a one dimensional lattice there is no critical point, because the long-ranged-ordered ferromagnetic phase is destroyed for any finite temperature. Long range order for finite temperatures first appears at dimension two. The dimension above which long range order first appears is called the lower critical dimension  $d_l$ , so that  $d_l = 1$  for the Ising model. At d = 2 and d = 3 the exponents which describe the second order transition from the ferromagnetic state to the paramagnetic state depend directly on the dimension. All systems with  $d \geq 4$  are in the same universality class and they are described correctly by the mean-field theory. (An introduction to the mean-field theory for statistical systems is given in the following chapter.) The dimension at which the mean-field theory becomes valid is called the upper critical dimension  $d_u$ .

Adding disorder: the Random Field Ising Model. In 1975 Y. Imry and S.-K. Ma published an epoch making paper [20] in which they demonstrated that the universality class of a system must also depend on another important effect, which should be common in many realistic systems: the presence of disorder. Imry and Ma introduced disorder to the Ising model in a rather formal way: They considered a ferromagnet, where at every site in the lattice there is a local magnetic field, which follows a random distribution. The random field does not vary in time and is therefore called "quenched" disorder in contrast to thermal disorder, which leads to fluctuations in time. This system is called the Random field Ising Model, or RFIM, and is modeled by the following Hamiltonian:

$$\mathcal{H} = -\sum_{\langle ij \rangle} JS_i S_j - \sum_i h_i S_i, \tag{1.1}$$

where  $S_i = \pm 1$  are Ising spins, the first sum goes over all interacting sites and the local magnetic fields  $h_i$  are independent random variables, which follow a distribution  $P(h_i)$  with zero mean value.

In their paper Imry and Ma present a short and emphatic argument why even an arbitrarily small random field must shift the lower critical dimension: The energy cost to flip a whole domain of a lattice without a field to opposite ferromagnetic order is determined by the size of the domain wall at which the ferromagnetic couplings have to be violated. For a domain of linear size  $\sim L$  the size of a domain wall in a d dimensional lattice is of order  $L^{d-1}$ . As soon as the random field is applied there is the probability that within this finite sized domain the local fields favor one spin direction even though in the mean over the whole lattice these effects cancel each other. These fluctuations are of order  $L^{d/2}$ , since the number of sites in the domain is of order  $L^d$ . Therefore for  $d \leq 2$  it will always be favorable for the ordered system to break into domains, so that the long-range ordered state becomes unstable even for zero temperature. Hence the lower critical dimension has to be greater than one. Since Imry and Ma's paper the RFIM has been one of must studied statistical systems. The new research field of disordered systems was born.

Dimensional reduction and the lower critical dimension of the RFIM. Four years after the Imry and Ma paper G. Parisi and N. Sourlas predicted a striking property of the RFIM [27]: The RFIM in d dimensions was claimed to be in the same universality class as the Ising model without disorder in d-2 dimensions. At that time this statement was in agreement with other results for the RFIM and one could immediately conclude that for the RFIM  $d_l=3$  and  $d_u=6$ . However, in 1984 J. Z. Imbrie published a paper [19] in which he showed explicitly that at zero temperature the long-range-order in the RFIM is stable for d=3 and weak random fields. Later, J. Bricmont and A. Kupiainen could show that this is also true for low finite temperatures [7], so that the lower critical dimension has to be two instead of three. That is the reason why the results of Sourlas and Parisi have been questioned.

Various renormalization group calculations, the first one by Aharony in 1978 [1],

have predicted the same results as the dimensional reduction. Thus, the renormalization group calculations contradict the explicit results for three dimensions. This contradiction has led to various attempts to explain why the renormalization group fails for the RFIM. There is still no generally accepted resolution to this problem.

The DAFF as an experimental realization of the RFIM. The theoretical discussions and disagreements about the RFIM has of course produced the desire among researchers for an experimental version of the RFIM. However, even though disorder is very common in natural systems it is not easy to find an Ising system where the disorder can be added in a controlled way. The random field which has been used in the theoretical model can of course not be realized in experiments. A paper by S. Fishman and A. Aharony [1] has led the way: They claim that the RFIM is in the same universality class as a randomly diluted antiferromagnet in a uniform magnetic field, the DAFF. (The Hamiltonian of the DAFF is introduced in section 1.3.1, eq. (1.3).) Later, J. L. Cardy has demonstrated this mapping in a different way and could even get an explicit expression for the effective random field in the DAFF in the limit of weak disorder [9]. A measure of the strength of the disorder in the DAFF is the dilution.

The most common experimental realization of a DAFF is the crystal  $Fe_cZn_{1-c}F_2$ . The Zinc ions in this crystal do not have an effective spin and hence cause the dilution.  $Fe_cZn_{1-c}F_2$  has the structure of a 3d BCC lattice and will be introduced in the following section. Other experimental systems are  $Fe_cMg_{1-c}Cl_2$ ,  $Co_cZn_{1-c}F_2$  or the 2d system  $Rb_2Co_cMg_{1-c}F_4$ . Experiments on these systems are an active field of research. A current review can be found in [5]. However, despite years of study there is no experimental phase diagram for the whole range of magnetic fields and dilutions.

#### 1.2 Outline and context of the work in this thesis

Compared to the huge number of publications of theoretical works on the RFIM, the number of theoretical works which consider directly the DAFF is relatively small. However, in this thesis we shall demonstrate that the DAFF for itself exhibits a very complex and interesting behavior and that the exact correspondence between the DAFF and the RFIM is not true in general.

The focus of this thesis is the DAFF in the low temperature regime. We study the DAFF at zero temperature by two different techniques:

- a mean-field theory on the Bethe lattice
- exact ground state simulation in three dimensions

These methods enable us to establish the phase diagram of the DAFF for the mean-field case as well as in three dimensions for the BCC and the cubic lattice. The variable parameters in the ground state are the applied magnetic field and the site dilution, which corresponds to the disorder. As a taste of the results we find, the phase diagram for the BCC lattice, which closely corresponds to the real system of  $Fe_cZn_{1-c}F_2$  is shown in figure 1.1

The story of the RFIM is a story full of misunderstandings. A striking result is that this phase diagram exhibits three different phases in contrast to the RFIM which just exhibits one phase transition at zero temperature. Between the antiferromagnetic state and the paramagnetic state there is an intermediate phase, which is called the domain state. This state has been predicted by a replica mean-field calculation [10] and local-mean-field studies [36],[29], [28] for the case of finite temperatures. (These results will be reviewed in detail in the following chapter.) By introducing an appropriate order parameter for the ground state we find that this

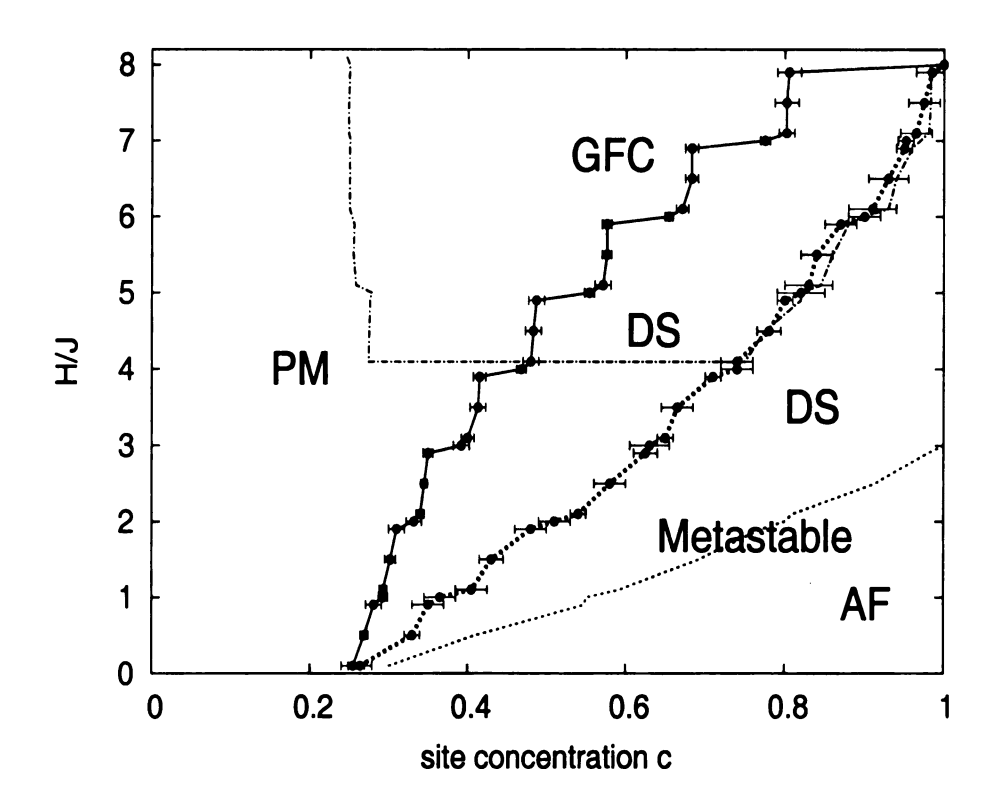


Figure 1.1: Phase diagram for the L=50 BCC lattice. AF stands for the antiferromagnetic phase, DS for an intermediate phase: the domain state, and PM for the paramagnetic state. GFC stands for the region in which there is a spanning ferromagnetic cluster. The x-axis shows the site concentration and the y-axis shows the applied magnetic field in units of the coupling strength J. A detailed discussion of this phase diagram is given in chapter 3.2.3

phase is also present in the case of zero temperature, in the mean-field limit as well as for the BCC and the cubic lattice.

However, recent studies of the 3d RFIM ground state have just found one phase transition. The variable parameters in the RFIM ground state is a uniform applied magnetic field and the variation of the random field, which corresponds to the disorder. In [30] E.T. Seppälä, A.M. Pulkkinen and M.J. Alava use percolation methods to construct a phase diagram which contains a ferromagnetic phase and a paramagnetic phase. Another work which states very clearly that there is just one phase transition in the RFIM ground state was published by A.A. Middleton and D.S. Fisher [25]. They also interpret the phase without long-range-order as paramagnetic without any glassy behavior. Studies of the RFIM ground state are supposed to reveal all the aspects of the low temperature behavior of the RFIM. This is due to a work of A.J. Bray and M.A. Moore [6] since which it is generally assumed that the low temperature regime of the RFIM is governed by a zero temperature fixed point.

The interpretations of the RFIM ground state phases stand in contrast to the results of a replica calculation by M. Mézard and R. Monasson [23]. They find that in the finite temperature regime the RFIM exhibits three different phases: the ferromagnetic phase, the paramagnetic phase and a glassy phase which displays replica symmetry breaking. Below a critical temperature the paramagnetic phase disappears, so that these results predict that there is only the ferromagnetic phase and a glassy phase in the ground state.

Other recent works which consider the DAFF ground state [17], [13] do not clearly distinguish three different phases, because they focus on order parameters which cannot distinguish between the domain state and the paramagnetic phase. In this thesis we introduce an order parameter, which can clearly distinguish three different phases in the DAFF ground state: the probability that a site is on the giant antiferromagnetic cluster. As mentioned above, this leads to results which are consistent with

previous studies of the DAFF at finite temperatures. By applying the same interpretation which we use for the DAFF to the results of Seppälä et al. [30] we argue that their interpretation of the phases is incorrect. What they consider as the paramagnetic phase actually corresponds to the domain state in the DAFF: a phase, which may exhibit spin glass features, so that the prediction from the replica calculation is correct. Many works on the RFIM implicitly assume that the RFIM ground state exhibits a ferromagnetic and a paramagnetic phase. These works have therefore to be reconsidered.

Finally, we can conclude that in the low temperature regime there is an important qualitative difference between the DAFF and the RFIM: In the low temperature regime the 3d DAFF exhibits a long-ranged-ordered phase, a glassy domain phase and a paramagnetic phase, whereas the 3d RFIM exhibits just the long-ranged ordered state and the glassy phase; the paramagnetic state appears only at finite temperatures.

Further results In agreement with the local-mean-field theory calculations we find indications for metastable states in the domain state and in the antiferromagnetic state. This raises the important question if the antiferromagnetic state can actually be realized in experiments. It would be very desirable to find observables which enable a reliable distinction of the different phases in the real systems. In particular, it may be quite difficult to distinguish the domain state from the antiferromagnetic state. A schematic study of  $Fe_cZn_{1-c}F_2$  for a the whole range of concentrations c in the low temperature regime could be directly compared to the presented phase diagram.

The concrete outline of this thesis is as follows: The following section 1.3 introduces some basic concepts which are necessary for an understanding of the further discussion. Basically, the main chapters also include comprehensive introductions to the methods which are applied so that they should also be understandable by non-

specialists.

Chapter 2 is concerned with different mean-field approaches to the DAFF. It starts with a general introduction to the mean-field theory and a basic derivation for the DAFF. Then the results of previous mean-field calculations are reviewed. Finally chapter 2 presents a new mean-field technique on the Bethe lattice. This technique is used to construct the mean-field phase diagram for the DAFF ground state.

Chapter 3 presents the results of exact ground state simulations for the DAFF. At the beginning an efficient algorithm for the DAFF ground state calculation is reviewed. This algorithm is then used for detailed studies of the cubic lattice and the BCC lattice, which lead to the final phase diagrams for these lattices.

Finally, the conclusion (chapter 4) picks up on the points from the introduction and clarifies our statements in the light of the new results.

#### 1.3 The basics

In this section I introduce the basic concepts, which I will use in the further discussion. The crystal structure of  $Fe_cZn_{1-c}F_2$  is related to the models of the DAFF, which are usually the starting point for all theoretical investigations. Then I give a brief review of the order parameters, which are used to characterize the different phases of the DAFF.

## 1.3.1 From the crystal structure of $Fe_cZn_{1-c}F_2$ to the DAFF Hamiltonian

 $FeF_2$  is a classical experimental realization of an Ising antiferromagnet. Each iron ion  $Fe^{2+}$  has an effective spin and is grouped with two fluorine ions  $F^-$ .  $FeF_2$  has a strong single ion-anisotropy, which breaks the spatial symmetry and creates one distinguished axis in the crystal. The spins of the iron ions align themselves along

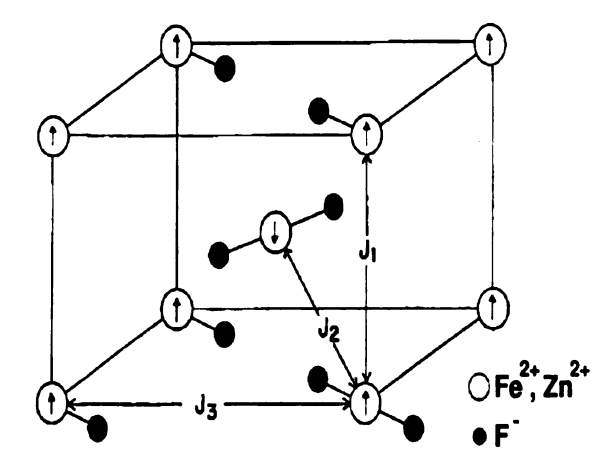


Figure 1.2: Schematic figure of one cell of  $FeF_2$ . The antiferromagnetic coupling  $J_2 = J_{AF}$  of all the outer Fe-ions with the Fe-ion in the center is dominant.  $J_1$  stands for the weak ferromagnetic coupling  $J_F$ ,  $J_3$  for the weak antiferromagnetic coupling  $J_{frust}$ . This figure has been taken out of [28]

this axis, which makes  $Fe_cZn_{1-c}F_2$  a nearly ideal Ising system, where every spin can have only two values: up or down. A basic picture of the crystal structure of  $FeF_2$  could be established by the neutron scattering experiments of Hutchings et al. in 1970 [18]. Figure 1.2 shows a schematic picture. The principal structure is a BCC lattice, which can be imagined as two cubic lattices, where the sites of one lattice are sitting in the center of the cubic cells of the other lattice.

The magnetic interaction between the spins of the Fe-ions can be described by three different nearest neighbor couplings. The dominant interaction is an antiferromagnetic coupling  $J_{AF}$  of each site with its eight neighbors on the surrounding cubic cell. Furthermore there is a weak antiferromagnetic coupling  $J_{frust}$  and weak ferromagnetic coupling  $J_F$  as illustrated in figure 1.2. Hutchings et al. have measured the ratios between the different couplings [18]:  $J_{frust}/J_{AF} = 0.053$  and  $J_F/J_{AF} = -0.013$ .

Disorder can be applied to this antiferromagnet in the form of dilution of the iron ions. In the dilution process Fe-ions are randomly substituted by zinc ions, which have no effective spin. The resulting crystal  $Fe_cZn_{1-c}F_2$  can be realized for any

concentration c of iron ions. High magnetic field experiments [21] have shown that the coupling strengths do not depend on the concentration c of magnetic ions.

Thus, all the essential magnetic features of  $Fe_cZn_{1-c}F_2$  in a magnetic field H are modeled by the following Hamiltonian:

$$\mathcal{H} = \sum_{\langle ij \rangle} J_{ij} \epsilon_i \epsilon_j S_i S_j - \mu_0 \sum_i \epsilon_i S_i H, \tag{1.2}$$

where the first sum goes over all lattice neighbors and  $J_{ij}$  is  $J_{AF}$ ,  $J_{frust}$  or  $J_F$ , depending on the coupling of the considered neighbors. The  $\epsilon_i$  represent the dilution.  $\epsilon_i$  is one if site i is occupied by a iron ion, whereas it is zero if site i is occupied by a zinc ion.

In theoretical physics it is common to choose the units of the coupling constants such that the spins take only the dimensionless values +1 or -1. The magnetic field is usually measured in units of the dominant coupling  $J_{AF}$ , so that  $\mu_0 = 1$ . The classical DAFF Hamiltonian, which is usually the basis for all analytical derivations, considers just one type of antiferromagnetic interaction:

$$\mathcal{H} = J \sum_{\langle ij \rangle} \epsilon_i \epsilon_j S_i S_j - \sum_i \epsilon_i S_i H, \tag{1.3}$$

where the sum goes over all nearest neighbor couplings. The number of neighbors with which one site interacts is called the *coordination number* of the lattice. If we only consider the dominant coupling of  $Fe_cZn_{1-c}F_2$ , then the coordination number is eight; for a cubic lattice it is six.

For  $FeF_2$  it is obvious that in the ground state not all magnetic couplings can be satisfied. The weak further neighbor bonds  $J_{frust}$  will be violated. The impossibility to satisfy all couplings is called *frustration*. The necessary condition to avoid frustration caused by nearest neighbor antiferromagnetic bonds is that the lattice is bipartite. A bipartite lattice can be divided in two sublattices, in such a way that no sites within the same sublattice are connected by an antiferromagnetic bond. Thus, if all spins of one sublattice are up and all spins of the other sublattice are down then all antiferromagnetic bonds are satisfied. If the weak antiferromagnetic bonds are neglected then the BCC lattice model of  $Fe_cZn_{1-c}F_2$  is also bipartite. Each sublattice is a cubic lattice. It is also easy to see that square and cubic lattice models with nearest neighbor interaction are also bipartite.

#### 1.3.2 Order parameters for the DAFF

The essential theoretical quantity which describes the macroscopic state of a statistical system is the order parameter. For a bipartite antiferromagnet the classical order parameters are the magnetizations of the two sublattices S1 and S2. The sublattice magnetization of S1 is

$$m_{S1} = \frac{2}{N} \sum_{i \in S1} \langle S_i \rangle, \tag{1.4}$$

where < ... > denotes the thermal average, N is the total number of sites and the sum goes over all sites in sublattice S1. The sublattice magnetizations can be combined to form the staggered magnetization:

$$m_{stagg} = \frac{m_{S1} - m_{S2}}{2},\tag{1.5}$$

which is a direct measurement for the antiferromagnetic order. In the ground state of an antiferromagnet without a field all spins of one sublattice will be down whereas all spins of the other sublattice will be up; the staggered magnetization is one. This is the *antiferromagnetic phase* which is determined by the existence of long-range-order.

At high temperatures the spins are flipping back and forth due to the thermal fluctuations. The thermal average of each spin is zero and therefore  $m_{stagg}$  is zero as

well. This is the *paramagnetic phase*, in which all order is destroyed by the thermal fluctuations.

The thermal average of the spin of a specific site i is called the local magnetization  $m_i = \langle S_i \rangle$ . One of the basic experiences from the investigation of disordered systems is that the sublattice magnetizations can be zero even though the local magnetizations are not zero; the spin configuration is stable against the thermal fluctuations, but it does not have long-range-order; only local order is present. This phenomenon has first drawn the attention of scientists in the seventies in the context of spin glasses. Edwards and Anderson have introduced an additional order parameter by which one can distinguish this phase from the paramagnetic state [12]:

$$q = \frac{1}{N} \sum_{i} m_i^2 \tag{1.6}$$

q is called the Edwards-Anderson order parameter.  $q \neq 0$  as long as the system is not in the paramagnetic state. A phase without long-range order but with  $q \neq 0$  is called a glassy phase or a spin-glass phase.

The discussion in this thesis focuses on the limit  $T \to 0$ : the DAFF ground state. The staggered magnetization can also be calculated in the ground state by simply averaging the spin values instead of the local magnetizations. But obviously the Edwards-Anderson parameter looses its significance. In the following chapter (section 2.4.3) I will introduce and motivate a new order parameter for the DAFF, which makes it possible to distinguish the different phases in the ground state: the probability that a site is in a giant antiferromagnetic cluster.

### Chapter 2

### Mean-field theory

The mean-field theory (MFT) approach belongs to the standard methods for the investigation of phase transitions in disordered systems. In this chapter I present a new mean-field technique and apply it to establish the phase diagram for the DAFF ground state. In order to put the results of this technique in the context of other mean-field approaches, this chapter also contains a general introduction and a review of past MFT treatments of the DAFF. The discussion within this chapter follows two main objectives: firstly, to combine the different MFT results to a coherent theoretical picture of the DAFF; secondly, to establish a new mean field technique, which can be applied in many other contexts. Therefore I will not only focus on the results of the other mean-field treatments of the DAFF, but also on the general techniques, to enable a comparison of the different approaches.

The outline of this chapter is the following: The first section gives a general introduction to the mean-field concept. In the second section I present an introductory MFT derivation for the DAFF. The validity of its final result is based on strong assumptions and is therefore very limited, but the derivation will demonstrate basic concepts and yield important results, which form the basis for the further discussion. In section 2.3 I review the methods and results of MFT calculations for the DAFF

in the literature. Finally, I will present the new MFT method, which is Bethe lattice MFT, in section 2.4. This method is then applied to DAFF ground state.

#### 2.1 Introduction to the mean-field approximations

The usual way to derive the behavior of a system in statistical physics is to minimize the free energy, which can be calculated from the partition function. However if one tries this approach for a disordered system like the DAFF, one will soon find that the problem becomes mathematical inextricable. The main purpose of the mean-field theory is to help out this unpleasant situation by applying reasonable approximations. The complex interaction structure of the system is substituted by a somewhat simpler "mean-field" interaction. The approximations, which have established themselves by yielding sensible results for different systems, can be subsumed into two categories:

- neglect of the thermal fluctuations of the order parameter
- neglect of the specific geometrical structure of the system

The first approximation type ignores the fluctuations of the order parameter X around its thermal average  $\overline{X}$ . Concretely this means that the Hamiltonian of the system is expressed in terms of  $\overline{X}$  and all terms of order  $\overline{(\overline{X}-X)^2}$  are neglected; the bar denotes of course the thermal average. This mean-field approximation can be seen at work in the next section, where I will apply it to the DAFF.

The second type of approximation neglects the specific geometrical structure of the system. Square, cubic and BCC lattice are lumped together and modeled by the same Hamiltonian. Instead of considering the real lattice, one derives the free energy for a substitute lattice. There are two common substitute lattices which enable an analytical treatment for many systems. The most commonly used model is the *infinite* range model: every site of the system is interacting with all other sites in exactly the same strength.

The other possible substitute lattice is the *Bethe lattice*, which is also called a *Cayley tree*. The Bethe lattice is used primarily in the context of percolation theory. It has the special property, that it has no loops, which makes it - as we will see - very suitable for probability considerations. I will give a detailed introduction to the Bethe lattice in section 2.4.1, where I present a new Bethe lattice MFT derivation. An introduction to the Bethe lattice in the context of percolation theory is given in [33].

The mean-field approximations have established themselves because they help to gain a lot of information about the system. The following experience from the investigation of critical phenomena is crucial: The results from MFT for the critical exponents become exact above a so called upper critical dimension  $d_c$ . The term "dimension" refers to the geometry of the system. For example, the dimension of the square lattice is two and for the cubic lattice it is three. Below the critical dimension there are dimensionality dependent correction terms to the mean-field results, but for most cases the existence and the nature of different phases is still predicted correctly. This dimension dependent validity can be explained theoretically by the renormalization group technique. For some systems like the Ising ferromagnet the renormalization group makes it also possible to calculate the upper critical dimension and the correction terms to the MFT results below the critical dimension. But there is no working renormalization group calculation for the DAFF or the RFIM.

Illustratively, one can try to imagine the dimension dependent validity of the MFT in the following way: with the dimension the connectivity of the lattice increases, e.g. every site is connected to four other sites in a square lattice and to six in a cubic lattice. A highly connected lattice is more similar to the infinite range model than a lattice with low connectivity. Fluctuations are less important, because every site is influenced by many different sites whose fluctuations average themselves out. Loops are less important, since the influence of a specific site on itself becomes small

compared to the increasing influence of other sites on it.

Which of the mean-field approximations is best to use depends in general on the system. In many cases different approximations can be applied to the same system and lead to equivalent results.

#### 2.2 Take I: A basic MFT for the DAFF

In the last section we have seen that there are different approaches to the mean-field theory of a system. In this section I will derive a mean-field theory for the DAFF which starts with the neglect of the thermal fluctuations (subsection 2.2.1). We will see that more assumptions are necessary to derive analytical results from the mean-field equations, and we will consider a bipartite lattice with uniform sublattice magnetizations (subsection 2.2.2). Finally, I will use the mean-field equations to establish the phase diagram in the limit of an infinite coordination number (subsection 2.2.3).

On our way we will encounter many links to MFT results for the DAFF in the literature. Thus, this derivation will provide a helpful basis for the further mean-field discussions, especially for the literature review (section 2.3).

#### 2.2.1 Neglect of the thermal fluctuations

We start with the DAFF Hamiltonian:

$$\mathcal{H} = \sum_{\langle ij \rangle} J\epsilon_i \epsilon_j S_i S_j - \sum_i H\epsilon_i S_i, \tag{2.1}$$

where the sum  $\langle ij \rangle$  goes over all lattice neighbors. The coordination number of the system is z, which means that every site has z neighbors, and the total number of sites is N. J > 0 is the coupling constant and H the applied uniform magnetic

field. The  $\epsilon_i$  represent the dilution. Thus their probability distribution is

$$P(\epsilon_i) = c\delta(\epsilon_i - 1) + (1 - c)\delta(\epsilon_i), \tag{2.2}$$

where c is the site concentration. In order to neglect the thermal fluctuations, we make the following ansatz:

$$S_i = m_i + (S_i - m_i), \tag{2.3}$$

where  $m_i$  is the thermal average of the spin value at site i. Plugging this ansatz into the Hamiltonian (2.1), we get

$$\mathcal{H} = \sum_{\langle ij \rangle} J\epsilon_{i}\epsilon_{j} (m_{i} + (S_{i} - m_{i})(m_{j} + (S_{j} - m_{j})) - \sum_{i} H\epsilon_{i}S_{i}$$

$$= J\sum_{\langle ij \rangle} \epsilon_{i}\epsilon_{j} (-m_{i}m_{j} + m_{i}S_{j} + m_{j}S_{i}) - \sum_{i} H\epsilon_{i}S_{i}$$

$$+ \mathcal{O}((S_{i} - m_{i})^{2}). \tag{2.4}$$

We will neglect the fluctuation terms  $(S_i - m_i)^2$ , so that the corresponding partition function becomes

$$Z = \text{Tr } e^{-\beta \mathcal{H}} = \sum_{\{S_i\}} \exp \left[ \beta J \sum_{\langle ij \rangle} \epsilon_i \epsilon_j m_i m_j - \beta \sum_i \left( \sum_{i \to j} J \epsilon_j m_j - H \right) \epsilon_i S_i \right]$$
 (2.5)

where  $\{S_i\}$  denotes the sum over all possible spin configurations and  $(i \to j)$  denotes the sum over all neighbors of i. Evaluating the first sum (2.5) becomes

$$Z = \exp\left(\beta J \sum_{\langle ij \rangle} \epsilon_i \epsilon_j m_i m_j\right) 2^N \prod_i \cosh\left[\epsilon_i \beta \left(H - \sum_{i \to j} J \epsilon_j m_j\right)\right]$$
(2.6)

Now we can calculate the thermal average of an existing spin  $S_i$  in the usual way:

$$m_i = \frac{1}{Z} \sum_{\{S_i\}} S_i e^{-\beta \mathcal{H}} = \tanh \left[ \beta \left( H - J \sum_{i \to j} \epsilon_j m_j \right) \right]$$
 (2.7)

We get a set of self consistent equations, one equation for every present lattice site. The solutions of these equations correspond to stable states of the system where the free energy has a local minimum. The equation set still contains the specific geometry of the system, since the sum  $(i \to j)$  over all neighbors of i takes the microscopical structure of the system into account.

In the so called local mean-field theory approach these equations are used as the basis for a numerical simulation. I will review this method and its results for the DAFF in section 2.3.2. Here I will now make further assumptions, so that we will loose the information about the magnetization of a single site i, but it will enable us to get more information about the system from analytic considerations.

#### 2.2.2 Further assumptions

In order to establish the phase diagram we are interested in the global order parameters of the system, for which we do not need the information about the microscopical magnetizations  $m_i$ . For the further derivations we will assume that the lattice, which we consider, is bipartite. As discussed in the introduction this means that we can divide it into two sublattices  $S_1$  and  $S_2$  in a way such that no sites which are in the same sublattice are connected to each other. The sublattice magnetizations  $m_{S_1}$  and  $m_{S_2}$  are then a natural measurement for the antiferromagnetic order of the system. The corresponding spatial fluctuations of the magnetizations,  $q_{S_1}$  and  $q_{S_2}$ , are important to determine the existence of a phase where the long range order is destroyed, but local order is still present. We can calculate these order parameters by averaging the mean field equations (2.7). Since both sublattices are equivalent, we can restrict

ourselves to sublattice S1.

$$m_{S1} = \frac{2}{N} \sum_{i \in S1} m_i = \frac{2}{N} \sum_{i \in S1} \tanh \left[ \beta \left( H - J \sum_{i \to j} \epsilon_j m_j \right) \right]$$
 (2.8)

$$q_{S1} = \frac{2}{N} \sum_{i \in S1} m_i^2 = \frac{2}{N} \sum_{i \in S1} \tanh^2 \left[ \beta \left( H - J \sum_{i \to j} \epsilon_j m_j \right) \right]$$
 (2.9)

In the expressions on the right hand side, the mean-field equations or the squared mean-field equations respectively are averaged over the whole lattice. The part of the mean-field equations (2.7) which varies from site to site is the sum over the neighbors  $\sum_{i\to j} \epsilon_j m_j$ . This sum depends on the number of neighbors, which are present and on the magnetizations of the present neighbors. In the lattice all of these configurations happen with a certain probability. Thus it is natural to calculate (2.8) and (2.9) by averaging over all possible configurations and weighting each configuration with its probability.

The problem is that we only know the probability distribution of the dilution coefficients  $\epsilon_i$ , but not of the magnetizations  $m_i$ . Therefore we will have to try an assumption. Let us assume that the sublattice magnetizations are uniform over the whole lattice:

$$m_{i} = \begin{cases} m_{s1} & \text{if } i \text{ is in sublattice 1} \\ m_{s2} & \text{if } i \text{ is in sublattice 2} \end{cases}$$
 (2.10)

In this way we neglect of course the spatial fluctuations of the magnetizations. The Edwards Anderson parameters  $q_{S1}$  and  $q_{S2}$  will go to zero, if  $m_{S1}$  and  $m_{S2}$  go to zero. This means that by our assumption we have already neglected the existence of a phase where only local order is present.

But now we can simplify equation (2.8). Since the sum  $\sum_{i\to j} \epsilon_j m_j$  in (2.7) always goes over the sites of the other sublattice, we can substitute  $m_j$  by  $m_{S2}$  and the

average becomes

$$m_{S1} = \int \prod_{k} d\epsilon_{k} (c\delta(\epsilon_{k} - 1) + (1 - c)\delta(\epsilon_{k})) \tanh \left(\beta H - \beta J \sum_{i \to j} \epsilon_{j} m_{S2}\right) =$$

$$= \sum_{k=0}^{z} \begin{pmatrix} z \\ k \end{pmatrix} (c)^{k} (1 - c)^{z-k} \tanh (\beta H - \beta J k m_{S2},)$$
(2.11)

where z is of course the coordination number. In this formula we encounter a binomial distribution. In order to simplify it, we can take advantage of the fact that, for a big number of Bernoulli trials, a binomial distribution can be approximated by a Gaussian distribution:

$$\begin{pmatrix} z \\ n \end{pmatrix} (c)^n (1-c)^{z-n} \to \frac{1}{\sqrt{2\pi\sigma^2}} \exp\left(-\frac{(n-cz)^2}{2\sigma^2}\right) dn \quad \text{for } z \to \infty, \tag{2.12}$$

where n has become a continuous variable,  $\sigma^2 = z(c)(1-c)$  is the variance, and pz is the mean value of the distribution. In practice this approximation becomes quite good for  $z \ge 6$ , which is already fulfilled for a cubic lattice. Thus we can apply it free of concerns:

$$m_{s1} = \int_{-\infty}^{\infty} dx \frac{1}{\sqrt{2\pi z c(1-c)}} \exp\left(\frac{(x-zc)^2}{2zc(1-c)}\right) \tanh\left(\beta H - \beta J x m_{s2}\right)$$
 (2.13)

Let us investigate this equation carefully, because it yields the first conclusions about our system. From our derivation it is easy to see that the corresponding mean field equation for an antiferromagnet without dilution is

$$m_{s1} = \tanh \left(\beta H - \beta \mathcal{J} z m_{s2}\right) \tag{2.14}$$

A comparison of (2.13) and (2.14) motivates the following interpretation of (2.13): The mean field equations for an antiferromagnet in a field are averaged over a Gaussian distribution of the coupling constants  $\mathcal{J}$ . Substituting  $x = \mathcal{J}z/J$  in the integral of (2.13) this becomes explicit, and we can see that the mean value of  $\mathcal{J}$  is cJ and the variance is  $c(1-c)J^2/z$ .

This result has already been found in a different way by Almeida and Bruinsma in [10]. They have used the *replica method* to show that in limit of high dimensions the DAFF is in the same universality class as a magnetic system with random couplings following the distribution derived above. I will give an introduction to the replica method and review Almeida's and Bruinsma's results in detail in section 2.3.1.

The result above already shows the limits of equation (2.13). A magnetic system with random exchange constants is in general a spin glass. Thus, we have to consider the possibility that the DAFF may have an additional phase in the phase diagram where the Edwards Anderson parameter is relevant. The sublattice magnetizations are not uniform in this phase. The replica solution of Almeida and Bruinsma [10] indeed contains the Edward Anderson parameters  $q_{S1}$  and  $q_{S2}$  and they show that the phase diagram exhibits a glassy phase.

#### 2.2.3 The mean-field phase diagram in the limit $z \to \infty$

We have lost the information about the spin glass phase by making assumption (2.10) which turns out to be not valid in the whole phase diagram. However, it should work in a special limit. The DAFF is equivalent to a system with random exchange constants, which have a variance of  $c(1-c)J^2/z$  and a mean value of cJ. In the limit of  $z \to \infty$  and for finite c the variance becomes negligible and the Gaussian

distribution can be substituted by a delta function. The coupling constants become uniform and thus the system is free of any quenched disorder. It is an accepted fact that systems without any quenched disorder do not exhibit a spin glass phase. Thus the assumption of a uniform sublattice magnetization becomes reasonable in the limit of infinite coordination numbers which corresponds to infinite dimensions or the infinite range model.

Before the replica calculation of Almeida and Bruinsma it was actually assumed that this approximation becomes already valid above d = 6. This assumption was based on a mean-field theory calculation for the RFIM by Aharony [1], though he did not derive them for the DAFF directly.

Since it will help to provide a basis for the further discussion, I will now use the mean-field equations to establish the phase diagram in that limit. Even though we will not be able to capture the glassy phase, we should get a sensible phase boundary for the transition from antiferromagnetic order to the paramagnetic phase.

Since we are now taking the limit  $z \to \infty$ , we have to ensure that the coupling constant is of order 1/z, so that the energy remains extensive. Thus we define  $J = J_0/z$ , where  $J_0$  is an intensive quantity. By approximating the Gaussian distribution by the delta function, the spatial fluctuations of the vacancies c(c-1) become irrelevant. Which means that we are now not only neglecting the thermal fluctuations but also all spatial fluctuations of the system. Equation (2.13) becomes:

$$m_{S1} = \tanh\left(\beta H - \beta c J_0 m_{S2}\right) \tag{2.15}$$

$$m_{S2} = \tanh \left(\beta H - \beta c J_0 m_{S1}\right) \tag{2.16}$$

Of course the equations for both sublattices are equivalent. Thus, we expect

degenerated solutions of the form  $m_{S1} = a$ ,  $m_{S2} = b$  and  $m_{S1} = b$ ,  $m_{S2} = a$ . Plugging (2.15) into (2.16) and dropping the sublattice index we get:

$$m = \tanh \left[\beta H - \beta c J_0 \tanh \left(\beta H - \beta c J_0 m\right)\right] \tag{2.17}$$

According to the degeneracy considerations this equation must have two solutions. For  $H < cJ_0$  they will have opposite signs and the staggered magnetization is the average of the absolute value of these two solutions. For H = 0 the magnetization of both sublattices is of course identical and  $m_{stagg} = m$ .

What can we learn from this equation about the phase diagram? Let us first consider the case of H=0. As the system goes from the antiferromagnet state to the paramagnetic state the magnetizations of both sublattices go to zero. Thus, we can expand (2.17) around m=0 to investigate the transition region:

$$m = (\beta c J_0)^2 m - 1/3 \left( (\beta c J_0)^4 + (\beta c J_0)^6 \right) m^3 + \mathcal{O}(m^4). \tag{2.18}$$

One can see that as  $m \to 0$ , a requirement for the consistency of (2.18) is that  $(\beta c J_0)^2 \to 1$ , and one can read off the critical temperature  $T_c = 1/\beta_c = c J_0$  at which the transition happens (for convenience the temperature is measured in units of the Boltzmann constant k).

Next we can determine the critical exponent  $\beta$ , which describes how the magnetization goes to zero at the critical point:

$$m = f(T - T_c)(T - T_c)^{\beta},$$
 (2.19)

where f is an arbitrary continuous function which does not go to zero for  $T \to T_c$ . Dividing (2.18) by m we can modify it to

$$m^{2} = \frac{3\beta^{2}}{(\beta cJ_{0})^{4} + (\beta cJ_{0})^{6}} (cJ_{0} + 1/\beta)(cJ_{0} - 1/\beta) \sim (T_{c} - T), \tag{2.20}$$

from which we can see that  $\beta = 1/2$ . It is not surprising that the results for  $T_c$  and  $\beta$  are the same as for an Ising ferromagnet, since an antiferromagnet on a bipartite lattice can be mapped to a ferromagnet whereby a uniform field becomes a staggered field (Section 3.1.3). Thus we only expect a difference as soon as we apply a finite field.

Let us investigate how the system behaves at  $T_c$  in a very small field. The exponent  $\delta$  describes how the magnetization goes to zero as  $H \to 0$ :

$$m = f(H)H^{1/\delta},\tag{2.21}$$

where f is again an arbitrary continuous function, which does not go to zero for  $H \to 0$ . Expanding (2.17) at H = m = 0 and  $\beta = 1/cJ_0$  yields

$$0 = -\frac{1}{3} \left( m + \frac{H}{cJ_0} \right)^3 - 1/3 \left( m - \frac{1}{3} \left( m + \frac{H}{cJ_0} \right)^3 \right)^3$$
 (2.22)

The first order terms in m and H cancel each other and we can see that  $\delta = 1$ . For a ferromagnet  $\delta$  is 3, which means that the m goes to zero more steeply.

To establish the phase diagram we would like to know the critical temperature also for nonzero values of the field. To calculate it we can use the following fact: at the transition point the staggered magnetization is very sensitive to any exterior influences on the system. An arbitrary small change of the field can lead to a finite jump in the magnetization. That is why the susceptibility  $\chi = \frac{\partial m}{\partial H}$  becomes infinite at the critical point. Taking the derivative of eq. (2.17) with respect to H on both sides and solving for  $\frac{\partial m}{\partial H}$  we get

$$\frac{\partial m}{\partial H} = \frac{\partial g(H, m)}{\partial m} / \left( 1 - \frac{\partial g(H, m)}{\partial m} \right), \tag{2.23}$$

where the right hand side of (2.17) has been denoted by g(H,m) and it has been taken into account that m is also a function of H. The susceptibility becomes infinite, if the denominator goes to zero. Thus, our condition for the critical point is

$$1 - (\beta c J_0)^2 \left( 1 - \tanh(\beta H + \beta c J_0 \tanh^2(-\beta H + \beta c J_0 m)) \right)$$
$$\times \left( 1 - \tanh^2(-\beta H + \beta c J_0 m) \right) = 0 \qquad (2.24)$$

For a fixed value of H, this equation still contains two variables m and  $\beta$ . As soon as a field is applied, the sublattice magnetization m is not necessarily zero at the critical point, because as soon as the antiferromagnetic order is lost the spins of both sublattices tend to align with the field.

We can investigate the qualitative behavior of the rhs of (2.24) by plotting it for different values of  $\beta$ . It has one maximum in m that lies in the region  $0 \le m \le 1$ . For big values of  $\beta$  the maximum value is negative for smaller  $\beta$  it becomes positive. Thus the critical point has to be the value of  $\beta$  at which the maximum value becomes zero, because this corresponds to the lowest temperature where we get for the first time a singularity in  $\chi$ . The value of m at which the rhs of (2.24) becomes maximal is the magnetization at the critical point.

The maximum can be calculated numerically. I have used Maple to calculate it stepwise for different temperatures and thus to find the temperature at which the maximum value becomes approximately zero. This has been done for varying values of H. The resulting phase diagram is shown in figure 2.1. It shows a paramagnetic and an antiferromagnetic phase. The information about the spin glass phase has been lost, but the phase diagram is correct for finite c in the limit of  $z \to \infty$ .

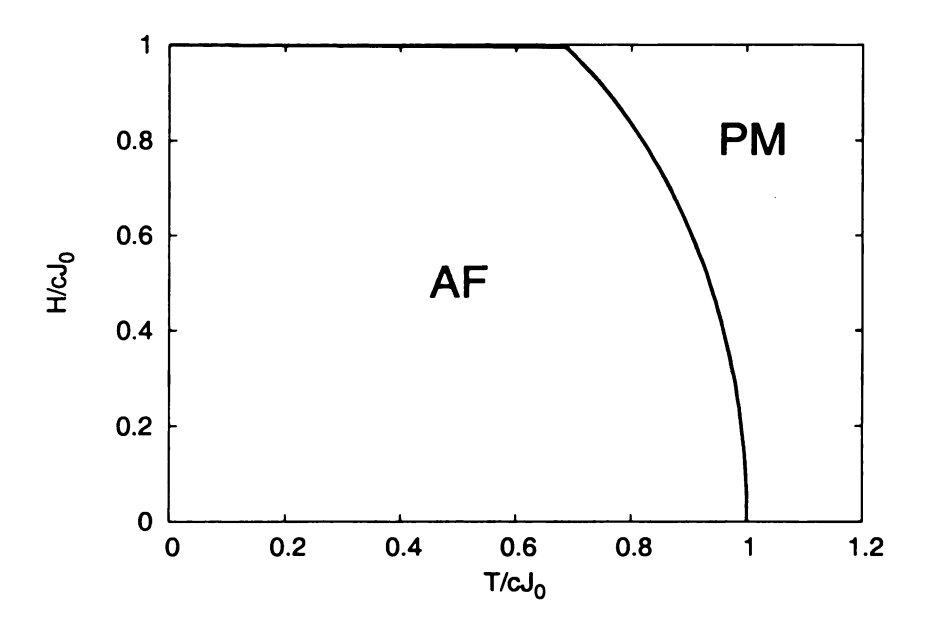


Figure 2.1: Phase diagram for the DAFF in the limit that the coordination number z goes to infinity.

# 2.3 Review of the mean-field calculations for the DAFF

The mean-field calculation in the last section was not sufficient to completely clarify all types of different phases of the DAFF. In the literature there have been two independent mean-field approaches, which are able to predict more details about the phase diagram. Firstly, there is the replica method, which has been applied to the DAFF in 1987 by Almeida and Bruinsma [10]. Secondly, there is a numerical approach, called local mean-field theory, which has been applied to the DAFF by three different groups [5],[29],[28].

Starting with the replica calculation I will first give an introduction to the general method and then review the actual results for the DAFF.

#### 2.3.1 The replica method

The replica method is a very common technique to derive the mean-field equations of systems with quenched disorder. It was first introduced by Sherrington and Kirkpatrick in 1975 [31] for the treatment of the infinite range Ising model with random exchange interactions, the theoretical paradigm of a spin glass. The essence of the replica method is a mathematical trick used to find the mean-field equations that are correctly averaged over the disorder.

In general the Hamiltonian of a disordered system contains parameters, which follow certain random distributions. In the case of the DAFF for example these are the dilution coefficients  $\epsilon_i$ . We have already seen in the last section that it is reasonable to average the mean-field equations over the random parameters. But in general this is a very critical task; in the last section we were only able to accomplish it by assuming a uniform sublattice magnetization, which is in general not true. The first step in the direction of the replica method is the idea to do the average not actually over the mean-field equations, but over the free energy function of the system. The mean-field equations can then be derived from the averaged free energy by minimizing it. One might ask why the average cannot be done at an even earlier stage over the Hamiltonian or the partition function. But it can quickly be checked that this leads to unphysical and simply wrong results. The reason is that the Hamiltonian and the partition function are non observable quantities which are connected to the final order parameters in a complex mathematical way. The assumption that the average over the free energy captures the essential physical features of the system is on the other hand simply justified by the successes of the replica method.

The next problem is that the average over the free energy  $F = -T \ln(Z)$  seems to be mathematical inextricable for all common random distributions. Here the replica trick comes into play. It uses the fact, that the logarithm can be expressed as the following limit:

$$\ln(Z) = \lim_{n \to 0} \frac{Z^n - 1}{n} \tag{2.25}$$

In the replica method it is now assumed that one can first average over  $\mathbb{Z}^n$  and then take the limit  $n \to 0$ . If n is an integer then  $\mathbb{Z}^n$  can be written as

$$Z^{n} = \sum_{\{S_{i}^{1}\}} \sum_{\{S_{i}^{2}\}} \dots \sum_{\{S_{i}^{n}\}} \exp\left(-\sum_{a=1}^{n} \beta \mathcal{H}[S_{i}^{a}]\right), \qquad (2.26)$$

where we have now n different sets of spins, so that we had to introduce an additional label a.  $\{S_i^a\}$  denotes the sum over all possible spin configurations of the  $a^{th}$  set. The different spin sets are called the replicas.

The average over an expression, which has the form of (2.26), can be done for many different cases of quenched disorder. Usually the expression can then be simplified, by using the Hubbard-Stratonovich transformation, which yields  $n^2$  new parameters.

The next steps are mainly based on intuition and their primary justification is the success of the results. Despite the fact that n has been restricted to integer values it is taken to zero. The question is what then happens to the  $n^2$  parameters. In their first solution Sherrington and Kirkpatrick have assumed a certain symmetry among these parameters, so that a parameter is either zero or has the same value q as all other non-zero parameters. This approach leads to mean-field equations, where the additional parameter q can be interpreted as the Edwards Anderson order parameter. This is called the replica symmetric solution.

Later in 1978 Almeida and Thouless [11] have shown that in the glassy phase with m = 0 and  $q \neq 0$  this solution becomes inconsistent. In many subsequent papers (a collection can be found in [24]) it is discussed how a different treatment of the  $n^2$  replica parameters, where the symmetry is broken and one gets more additional order parameters, can avoid this inconsistency.

At this point one can see the major weakness of the replica method. It depends

on elaborate mathematical operations, which are not all well defined and there are also no physical reasons to justify them. The solution depends on the treatment of the replica parameters, for which there is no unique or formal way, so that it has to be based on ad hoc assumptions. Still the replica method was very successful in making correct predictions, and has become a common tool for mean-field derivations in systems with quenched disorder. For Sherrington and Kirkpatrick's infinite range model a method of replica symmetry breaking has been developed, which leads to sensible results [24]. But even the symmetric solution can be very useful, especially to establish the phase diagram. In the paramagnetic phase the symmetric solution is consistent and describes the system accurately. The behavior of the system is predicted wrongly and the symmetric solution becomes invalid only in the glassy phase. That is why the inconsistency of the symmetric solution has been established as one of the theoretical indicators for a spin glass phase. One can find the phase boundary by looking for the breakdown line of the symmetric solution. In spin-glasses in an applied field this phase boundary is called the Almeida-Thouless line.

#### Almeida and Bruinsma's symmetric solution of the DAFF

A replica symmetric mean-field theory for the DAFF has been derived by Almeida and Bruinsma in 1987 [10]. Before their calculation it was assumed that above d=6 systems, which are in the RFIM universality class like the DAFF, do not exhibit a spin glass phase. This assumption was based on renormalization group arguments and a mean-field theory for the RFIM by Aharony [1]. The mean-field theory, which Aharony presents in [1], is equivalent to the mean-field theory, which I have derived in section 2.2.3 directly for the DAFF. We have already seen that this theory becomes valid for  $cz \to \infty$ , which corresponds to infinite dimensions. In [10] Almeida and Bruinsma argue that as long as the coordination number z remains finite this mean-field theory is not exact. Even above d=6 the DAFF exhibits a spin glass phase.

They show this by deriving a replica symmetric mean-field theory directly for the DAFF. Instead of the site diluted case, which is realized in the experimental systems, they consider the bond diluted case:

$$\mathcal{H} = \sum_{\langle ij \rangle} J_{ij} S_i S_j - \sum_{i} H \epsilon_i S_i, \qquad (2.27)$$

where the probability distribution of the  $J_{ij}$  is

$$P(J_{ij}) = c\delta(J_{ij} - J_o/z) + (1 - c)\delta(J_{ij})$$
(2.28)

Almeida and Bruinsma calculate the free energy by the replica method. Their mean-field approximation is to assume big but finite values of z. That is what allows them to make an expansion of the free energy up to the second order in  $(\beta J_0/z)$ . They find that this free energy is the same as for a system with random exchange interaction with a mean value  $\langle J_{ij} \rangle = J_0$  and variance  $\sigma^2 = c(1-c)(J_0/z)^2$ . We have already seen this result in a different way from our interpretation of equation (2.13).

By minimizing the free energy Almeida and Bruinsma derive the following meanfield equations:

$$m_{S1,S2} = \frac{1}{\sqrt{2\pi}} \int dx \ e^{-x^2/2} \times \tanh \left[ \beta \left( H - cJ_0 m_{S2,S1} + \sqrt{\frac{c(1-c)}{2z}} J_0 x \sqrt{q_{S1,S2}} \right) \right]$$
(2.29)

$$q_{S1,S2} = \frac{1}{\sqrt{2\pi}} \int dx \ e^{-x^2/2}$$

$$\times \tanh^{2} \left[ \beta \left( H - cJ_{0}m_{S2,S1} + \sqrt{\frac{c(1-c)}{2z}} J_{0}x\sqrt{q_{S1,S2}} \right) \right]$$
 (2.30)

One can see that in the limit  $z \to \infty$  these equations become equivalent to (2.15) and (2.16). But for finite z they contain explicitly the Edwards-Anderson parameter for both sublattices. Since these equations follow from a symmetric replica calculation, they become invalid in the spin glass phase. Investigating the mean-field equations and looking for the region, in which the symmetric solution becomes inconsistent, Almeida and Bruinsma establish the Almeida and Thouless line and the paramagnetic phase boundary. Their results are shown in figure 2.2.

## 2.3.2 Local mean-field theory

In the previous section we have seen that with the help of the replica method Almeida and Bruinsma could show analytically that the DAFF phase diagram exhibits a spin glass phase. In this section I will review a mean-field approach to the DAFF, which is mainly based on a numerical procedure: the local mean-field theory (LMF). A big advantage of this method is that it can reveal details about the system on the microscopic level. Thus it will help us to shed light on a question, which has been left unanswered by the replica calculation: What does actually happen in the glassy phase? What does it look like?

Another advantage of the local mean-field theory is that it can take many specific details about the system into account. Coutinho-Filho and Raposo for example have done local mean-field simulations, which consider the special crystal structure of  $Fe_xZn_{1-x}F_2$ , the most common experimental realization of a DAFF [28]. Earlier simulations for a DAFF on a regular cubic lattice have been done by Belanger et al. [36] and by Soukoulis et al. [29]. I will review these results after I have given a general introduction to the local mean-field theory concept.

In section 3.3 I will present a direct comparison of local mean-field simulations to

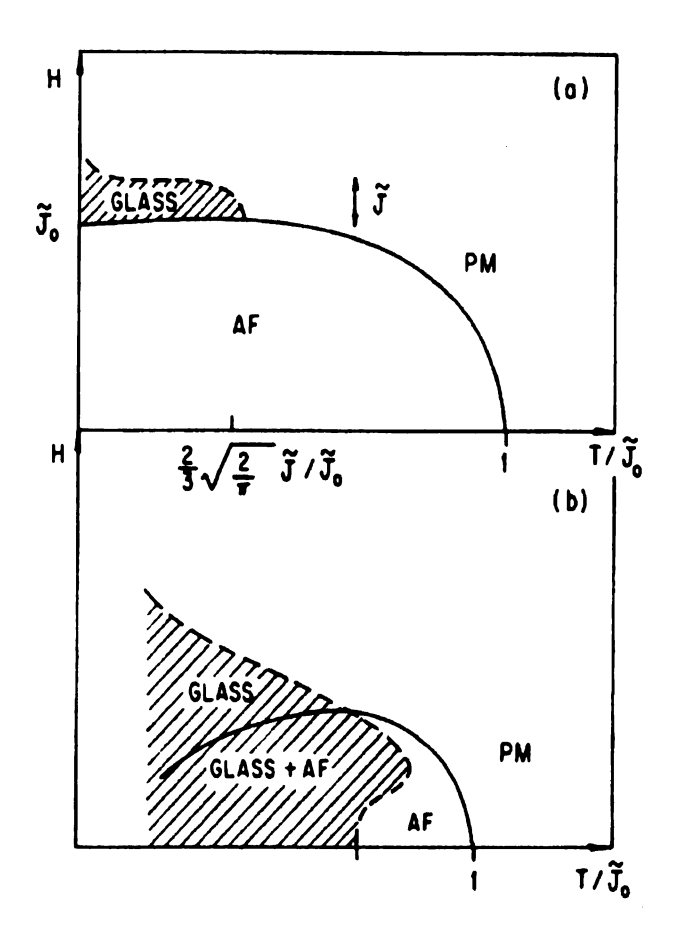


Figure 2.2: Phase diagram from the replica calculation with  $\tilde{J}_0 = cJ_0$  and  $\tilde{J} = \sqrt{c(1-c)/2z}J_0$ . Part (a) shows the case of low dilution. Part (b) for higher dilution. [10]

the exact ground state of the DAFF.

#### The local mean-field concept

The local mean field theory method has first been introduced by von Boehm and Bak in the context of modulated magnetic systems [34]. It has first been applied to disordered magnetic systems by Soukoulis et. al. in 1983 [16]. The basic idea is to solve the mean field equations of the form of (2.7) numerically by iteration:

$$m_i^{(n)} = \tanh \left[ \beta \left( H - J \sum_{i \to j} \epsilon_j m_j^{(n-1)} \right) \right] \quad i = 1 \dots N,$$
 (2.31)

where the index n counts the number of iterations. These equations still contain the specific geometric structure of the system, since there is an equation for every single site and the sum  $(i \to j)$  goes over all neighbors of this site. Of course similar equations can be derived quickly for all different kinds of magnetic systems by using the same ansatz as in section 2.2.1.

Starting with an arbitrary set of  $m_i^{(1)}$  and applying the iteration procedure (2.31) a sufficient number of times the values of the magnetizations  $m_i$  will converge to a stable value. Soukoulis has found in [16] that the iteration converges much faster, if one updates the values of the magnetizations immediately and not only after one iteration step is complete. This usually leads to the same results. After one complete iteration step the convergence can be checked by the following criterion:

$$\frac{\sum_{i=1}^{N} \left( m_i^{(n)} - m_i^{(n-1)} \right)^2}{\sum_{i=1}^{N} \left( m_i^{(n)} \right)^2} < \epsilon, \tag{2.32}$$

where one chooses finite but very small values of  $\epsilon$ , which determines the accuracy of the convergence. The resulting  $m_i$  are an approximate solution of the mean-field equations and thus should be a stable point of the system. But here one has to be very careful. It is a general feature of disordered systems, which exhibit a glassy phase, that their free energy landscape is very complex and fine structured. The free energy function has a huge number of local minima, which correspond to stable or metastable states of the system. The number of stable states in Sherrington and Kirkpatrick's infinite range model, which has been mentioned in the last section, for example increases exponentially with the size of the system [24]. Thus the solution of the iteration procedure is not unique and does depend strongly on the initial conditions: the starting value of the iteration  $m_i^{(0)}$ . So how can it then be ensured

that solutions are found, which correspond to the real physical system?

Boehm and Bak [34] have found a natural answer to that question. If the temperature of the system of the system is very high and the system is well in the paramagnetic phase, then the local magnetizations  $m_i$  will be very small and completely random. Thus, one should start in the high temperature phase with random starting values of the  $m_i$ . Then one can "cool down" the system in small temperature steps  $\Delta T$ . This means that one takes the solution of the higher temperature iteration as the starting value for an iteration where the temperature is slightly lower. This corresponds to a real cooling process. The temperature of the system is suddenly slightly decreased so that it is not in equilibrium any more. It is then allowed to come to equilibrium again, which is ensured by iterating until the convergence criterion is fulfilled. After cooling the system to minimal temperature it can be heated again in the same way. The results of the LMF for the DAFF [29], [36], [28] show that, if one chooses the temperature steps  $\Delta T$  and the value of  $\epsilon$  sufficiently small, then the final state after the cooling procedure does not depend any more on the random initial conditions.

By applying this procedure the numerical calculations simulate what is actually done in the real experiments. In the experiments the system is first cooled down and the measurements are then taken, when it is reheated again. For systems in a magnetic field there are two different ways of cooling. The first one is zero-field cooling, where the field is only applied after the cooling procedure is finished. The second one is field cooling, where the field is also applied during the cooling process. Of course both methods lead in general to different results, since the system may evolve to a different local minima in the free energy.

For the DAFF the LMF has been very successful in predicting results that coincide with the experimental ones. I will now review these results in detail.

#### LMF results for the DAFF

Two very similar local mean-field calculations for the DAFF have been done by Yoshizawa and Belanger in 1984 [36] and by Ro, Crest, Soukoulis and Levin and Levin in 1985 [29]. Yoshizawa and Belanger have studied the DAFF on a square, cubic and hyper-cubic (d=4) lattice. Soukoulis and coworkers have investigated the DAFF on a BCC lattice in three dimensions and the RFIM on a cubic lattice. Later in 1998 Coutinho-Filho and Raposo have done a LMF, which simulates the exact crystal structure of  $Fe_xZn_{1-x}F_2$ . I will start with the review of the older results, where I will focus especially on the calculations for the three-dimensional DAFF.

The results of Belanger and Soukoulis for the 3d DAFF The BCC lattice, which Soukoulis et. al consider has a size of  $2 \times 30^3$  and they focus on concentrations close to c = 0.7. The main focus of Belanger et al. in [36] is the square lattice, but they also consider  $12^3$  and  $18^3$  cubic lattices. Both investigate the final local magnetizations at different temperatures after they have done the cooling procedure, which I have described above. They consider field cooling as well as zero-field cooling at varying values of the magnetic field.

Both Belanger et al. and Soukoulis et al. find that the local magnetization patterns, which they get for different parameters of H, T and c, can be divided into three different categories. First there is the paramagnetic state where the local magnetizations are very small and randomly distributed. Then there is of course the state of long range order, where the magnetizations  $m_i$  are all positive on one sublattice and negative on the other sublattice. In the third state the lattice is divided in domains of opposite antiferromagnetic order. At the boundaries of these domains the antiferromagnetic order scheme is violated. The local magnetizations of neighboring sites have the same direction. This state is called in both papers the domain state or the multi-domain state.

The state of the system does not only depend on its current parameters of H, T and c but also on its history. If the temperature is below a critical temperature  $T_c$  and the magnetic field is below a critical value  $H_c$ , which depends on the dilution, then the long-range-order state has the lowest free energy. But the system will only evolve into that state if it is cooled in zero field. In the field cooling procedure the system will remain in the domain state, even if it is cooled below  $T_c$ . The system is captured in a local free energy minimum, which is not the global minimum. If the zero-field cooled system is heated then it will change into the domain state at a not uniquely determined temperature which lies above  $T_c$ . If the system is heated above a temperature  $T_N$  the system will change into the paramagnetic state, independent on its history.

A systematic study for a wide range of values for c and H is not presented in these papers. The phase diagram which Soukoulis et al. establish for c=0.7 is shown in figure 2.3.

Now let us connect these results to those from the previous sections. The domain state corresponds obviously to the spin glass phase, which Almeida and Bruinsma have found. The total sublattice magnetizations are zero, since the sublattice magnetizations have opposite signs within the different domains. But the Edwards Anderson order parameter is not zero and the system is locally ordered. Comparing figure 2.2 with figure 2.3 we can see that the phase diagrams are qualitatively similar.

The local-mean field theory results claim some interesting new features about the phase diagram. The glassy phase and the long-range-ordered phase are metastable, in the sense that within these phases the actual state of the system is history dependent. The long-range-order phase can only be reached by zero-field-cooling. Furthermore we get a picture of what the spin glass phase actually looks like. Domains of opposite antiferromagnetic order are inter-penetrating each other. We will learn more about the structure of these domains from the numerical ground state calculations in the

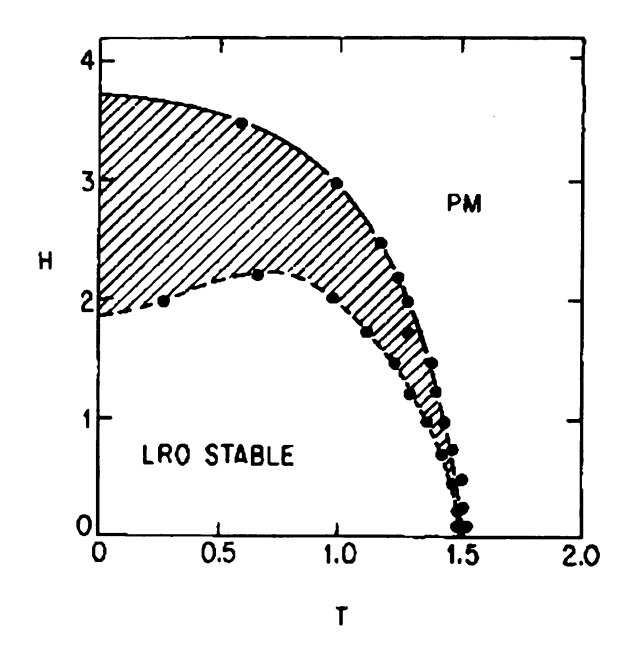


Figure 2.3: Phase diagram from the LMF calculation for a BCC lattice with c = 0.7. The shaded region marks the domain state. Transformed to our notation H is measured in units of 2J, and T is measured in units of 2k. [29]

next chapter. From now on I will speak of the domain phase or of the glassy phase with the same meaning.

Raposo's and Coutinho-Filho's results for  $Fe_xZn_{1-x}F_2$  In 1998 Raposo and Coutinho-Filho have published a local mean-field study [28], which models the crystal structure of  $Fe_xZn_{1-x}F_2$ , which has been presented in section 1.3.1. It is a BCC lattice with a dominant antiferromagnetic coupling  $J_{AF}$ . The special feature of  $Fe_xZn_{1-x}F_2$  is, that there are additional couplings  $J_F$  and  $J_{frust}$  with the next nearest neighbors, which are weak compared to the dominant coupling  $J_{AF}$ . The first additional coupling  $J_F = -0.013J_{AF}$  is ferromagnetic, but the second  $J_{frust} = 0.053J_{AF}$  is antiferromagnetic and therefore causes frustration. How these couplings are situated geometrically can be seen in figure 1.2 in section 1.3.1.

The mean field equations of the "pure" bipartite DAFF (2.7) can easily be adjusted

to the  $Fe_xZn_{1-x}F_2$  case. All one has to do is to include the additional bonds in the sum over the neighbors:

$$m_i = \tanh \left[ \beta \left( H - J_{AF} \sum \epsilon_j m_j - J_{frust} \sum \epsilon_j m_j + J_F \sum \epsilon_j m_j \right) \right],$$
 (2.33)

where the sums go of course over all neighbors, which are connected by the corresponding bonds.

Before Raposo's and Coutinho-Filho's results it was mainly believed that the frustration couplings are too weak to have a distinct influence on the phase diagram. One of the main issues of Raposo et al. is to show that this belief is wrong. They study a  $2 \times 30^3$  lattice in the whole range of concentrations c. Their study is very extensive and I will focus on their results for the low temperature regime.

They are cooling down the system to  $T=0.06\,T_N$ , where  $T_N$  is the temperature, above which the system becomes paramagnetic in the non-diluted case. They find that even at H=0 the system will go into the domain phase below the concentration c=0.63. This does not happen in the pure antiferromagnet, therefore the reason has to be the additional frustration bonds. Let us denote by  $H_{max}$  the field, which is necessary to break the antiferromagnetic order at low temperatures in a non-diluted lattice. For zero-field cooling with a field  $H=0.3H_{max}$  the behavior is exactly the same as for the H=0 case. The system will evolve into the domain phase, if the site concentration is smaller than c=0.63. Upon field cooling with the same field the system behaves differently. Domains of opposite antiferromagnetic order start to nucleate at concentrations c=0.94. The size of these domains increases slowly as the concentration is reduced. Only at c=0.5 the domains of opposite order become about the same size.

The natural conclusion of Raposo and Coutinho-Filho is that at zero-field cooling

the frustration bonds play an important role. Their influence is responsible for the critical concentration, below which the system evolves into the domain state. In the field cooling procedure on the other hand the effects of magnetic field are dominant and the frustration bonds have no notable influence on the system.

It is important to keep this result in mind, when one compares results that have been derived for the pure bipartite DAFF with the results of experiments on the real DAFF, where the weak frustration bonds play a role. In chapter 3 I will investigate the DAFF ground state on a bipartite lattice and so we have to be aware that this model only captures the critical behavior in the real DAFF system, that is due to the exterior field.

## 2.4 Take II: A Bethe lattice MFT for the DAFF

The mean-field approaches which have been presented in the previous sections have helped to develop a basic picture of the different phases of the DAFF. However, it is not clear how well the mean-field results describe a real system of a specific dimension. In the following chapter I will use computer simulations to establish the correct phase diagram for three dimensions for the case of zero temperature. Of course we would like to compare these exact results to the mean-field predictions. But the mean-field approaches, which have been presented so far break down in the limit  $T \to 0$ . That is why in this section I present a new mean-field ansatz, which works especially well for the case of T=0: a mean-field theory on the Bethe lattice. The special structure of the Bethe lattice has already been applied to derive the mean field equations for other magnetic systems. Hartmann and Zittarz have used it for calculations on the Ising model of a ferromagnet[26] and Bruinsma has applied it to the RFIM [8]. They all start by calculating the partition function. I present a different approach, which directly derives the self consistent equations for the order parameter. I will start

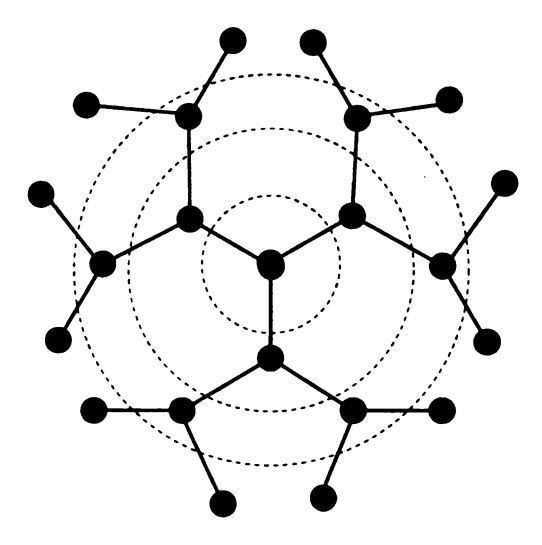


Figure 2.4: Bethe lattice with z=3. The dotted circles separate the different levels

with a general ansatz for finite temperatures in order to compare the results to the replica calculation (section 2.4.2). I will then focus on the limit  $T \to 0$  and use the same ansatz to derive the mean field equations for the appropriate order parameter of the DAFF ground state (section 2.4.4). As a preparation I will first introduce the Bethe lattice. A general introduction to the Bethe lattice in the context of percolation theory can be found in [33].

#### 2.4.1 The Bethe lattice

The Bethe lattice is an artificial structure, which in some sense corresponds to a lattice of infinite dimensions. It has become important in physics, because many problems, that cannot be solved exactly on the real crystal lattices, can be solved on the Bethe lattice. The Bethe lattice can be constructed with any coordination number z. Figure 2.4 shows a Bethe lattice with z=3.

The Bethe lattice can be described by the following construction rules: One starts with one site in the center and connects it to z newly created nodes. These nodes are at the surface level. Each single node at the surface level has now to be connected

to  $\alpha=z-1$  nodes, which are again newly created. These new nodes form the new surface level. Now one can continue to increase the size of the lattice by iterating the last step. If the size of the lattice goes to infinity, then the center of the lattice looses its distinguished position and every site can be taken as the center.  $\alpha=z-1$  is called the branching number of the lattice. The Bethe lattice can be divided into levels, where one level contains the nodes, that were created during the same iteration step. A single branch that leaves from the center site has the structure of a tree. That is why the Bethe lattice is also called a *Cayley tree*.

Now in what sense does this lattice correspond to infinite dimensions? The first corresponding feature is that in the Bethe lattice the mass of the sites is located at the surface. For  $z \geq 3$  there are more sites at the surface level, than in the rest of the lattice. For a hyper-cubic lattice the fraction of sites at the surface becomes only comparable to the site within the lattice as d goes to infinity, since the volume is of order  $L^d$  but the surface is of order  $L^{d-1}$ .

The second feature is that the Bethe lattice contains no loops. A loop is a path, that starts and ends at the same site and uses no bonds twice. A good illustration, why the loops on a regular lattice become negligible as  $d \to \infty$  can be found in [33]: For high dimensions d the number of ways to embed a chain of four sites on a hypercubic lattice is proportional to  $(2d-1)^3$ . However, the number of ways to form a loop, where all four sites have to be on the same plane is d(d-1). Therefore the loops become unimportant when  $d \to \infty$ . As we shall soon see these features are also the reason, why the Bethe lattice is so useful.

## 2.4.2 MFT ansatz for finite temperatures

The main purpose of this whole section is to derive a mean-field theory for the DAFF ground state. However, the new mean-field method for the Bethe lattice, which is introduced below can also be applied to the case of finite temperatures. Since the

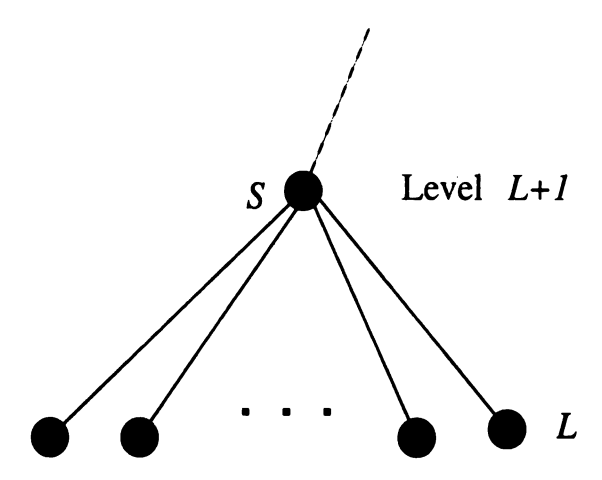


Figure 2.5: Illustration of the bonds of site s in the Cayley tree.

method itself is of interest, I will first demonstrate the general ansatz and compare the results to the replica solution, even though this does not lead to a directly solvable set of equations.

How can we take advantage of the special features of the Bethe lattice to derive the mean-field equations? We will make the following ansatz: At every site in the lattice we will consider the probability P that the site has spin up and the probability M=1-P that the site has spin down. The local magnetization of this site is then naturally m=P-M. Every site is connected to one site on the level above and to  $\alpha=z-1$  sites on the level below, as shown in figure 2.5.

This motivates the following assumption. We consider again the case of high coordination numbers, so that the influence of the one site on the upper lever becomes negligible and the spin of the regarded site is completely determined by the  $\alpha$  sites on the level below. This means that we can propagate the order of the spins up the Cayley tree. We should of course keep in mind that this approach is only made possible by the special structure of the Cayley tree. If the mass of the spins were not at the surface or if there were loops in the lattice, then this "one-way" determination of the spin order would not be possible.

Let us consider a single site s on level L+1, which is connected to  $\alpha$  sites on the level L below. Let us furthermore assume, that  $n \leq \alpha$  of these sites on level L are present and that k of them have their spin in the up direction. To ensure again that the energy is extensive J has to be of order  $(1/\alpha)$ . Now we can use the Boltzmann distribution to calculate the probability  $P_{L+1}$ , that s has spin up:

$$P_{L+1}(2k-n) = \frac{\exp(-\beta[(2k-n)J-H)]}{\exp[-\beta((2k-n)J-H)] + \exp[\beta((2k-n)J-H)]}$$

$$= \frac{\exp[-\beta((2k-n)J-H)]}{2\cosh[-\beta((2k-n)J-H)]}$$
(2.34)

The probability depends on the difference of the number of up spins k and the number of present spins n. n varies from site to site within the lattice. k varies even for one site due to the thermal fluctuations. To get rid of this dependence we will average  $P_{L+1}$  over all possible values of n and k. Naturally every configuration is weighted with its probability. For a given value of n the probability to have k up spins is  $(P_L)^k(1-P_L)^{n-k}$ , where  $P_L$  is of course the probability for a single spin being up on level L; the degeneracy of this configuration is n over k. The probability that n sites are present is  $(c)^k(1-c)^{\alpha-k}$ , where c is again the probability that a single site is present; and the degeneracy is  $\alpha$  over n. Hence the average over  $P_{L+1}(2k-n)$  is:

$$P_{L+1} = \sum_{n=0}^{\alpha} {\binom{\alpha}{n}} \sum_{k=0}^{n} {\binom{n}{k}} c^{n} (P_{L})^{k} (1 - P_{L})^{n-k} (1 - c)^{\alpha - n} \times \frac{\exp[-\beta((2k - n)J - H)]}{2\cosh[-\beta((2k - n)J - H)]}$$
(2.35)

We can do exactly the same procedure for the probability that s has spin down

 $M_{L+1} = 1 - P_{L+1}$  and obviously we will get exactly the same result as in (2.35) except for a different sign in front of the Boltzmann factor. Thus, the magnetization of s:  $m_{L+1} = P_{L+1} - M_{L+1}$  becomes

$$m_{L+1} = \sum_{n=0}^{\alpha} \binom{\alpha}{n} \sum_{k=0}^{n} \binom{n}{k} c^{n} (P_{L})^{k} (1 - P_{L})^{n-k} (1 - c)^{\alpha - n} \times \tanh\left[-\beta((2k - n)J - H)\right]$$
(2.36)

In this formula we encounter an average over two inter-weaved binomial distributions. In section 2.13 we have already used the fact that a binomial distribution can be approximated by a Gaussian distribution. The number of Bernoulli trials for the first distribution is  $\alpha$ , which we consider to be big. For the second distribution the number of trials n varies around the mean value  $c\alpha$  with fluctuations of order  $\sqrt{\alpha}$ . Thus for big values of  $\alpha$  and high and medium dilutions we can approximate both distributions by Gaussian distributions. The variance of the first distribution is  $\sigma_c^2 = \alpha(c)(1-c)$ . The second distribution has a mean value of  $nP_L$  and a variance  $\sigma_{P_L}^2 = n(P_L)(1-P_L)$ . Thus (2.36) becomes

$$m_{L+1} = \frac{1}{2\pi\sigma_c\sigma_{P_L}} \int dy \exp\left(-(y - \alpha c)^2/2\sigma_c^2\right) \int dx \exp\left(-(x - yP_L)^2/2\sigma_{P_L}^2\right)$$

$$\times \tanh\left[-\beta((2x - y)J - H)\right] (2.37)$$

where  $\sigma_{P_L}^2 = y(P_L)(1 - P_L)$  depends of course on y. But by expanding the denominator of the second exponential around the mean value of y, one sees that the linear term is already of order  $1/\alpha^2$ . This term is negligible against the constant term of order  $1/\alpha$ , so that we can ignore the fluctuations of the fluctuations:

$$\sigma_{P_L}^2 \approx c\alpha(P_L)(1-P_L).$$

x varies according to a normal distribution around mean value  $p\alpha$ . y also varies according to a normal distribution around yP, which varies itself. Intuitively it is clear that the difference of these to quantities (2y-x) should also vary like a normal distribution around the reasonable mean value  $c\alpha(2P-1)$ . For everybody, who does not believe in intuition, this can also be shown formally: Making the two-dimensional coordinate transformation  $\chi = 2y-x$  and  $\mu = 2y+x$  the hyperbolic tangent becomes independent of the second integration variable  $\mu$ . And one can now do the integral over  $\mu$ . Accomplishing all these calculations carefully - not forgetting the factor  $\frac{1}{4}$  from the coordinate transformation - we finally get:

$$m_{L+1} = \frac{1}{\sqrt{2\pi\sigma_{\chi}^2}} \int d\chi \, \exp\left(-\frac{(\chi - c\alpha(2P_L - 1))^2}{2\sigma_{\chi}^2}\right) \tanh\left[\beta(H - \chi J)\right], \quad (2.38)$$

where the new variance is  $\sigma_{\chi}^2 = 4\sigma_{P_L} + (2P_L - 1)^2\sigma_c^2$ .  $2P_L - 1 = P_L - M_L$  can be substituted by the magnetization on level L,  $m_L$ . Obviously the Bethe lattice is bipartite: level L + 1 belongs to one sublattice and level L to the other sublattice. Assuming that the magnetizations are independent of the specific level we can define  $m_{S1} = m_{L+1}$  and  $m_{S2} = m_L$ . Making one further coordinate transformation (2.38) finally becomes

$$m_{S1} = \frac{1}{\sqrt{2\pi}} \int dx \, e^{-1/2x^2} \times \tanh \left[ \beta \left( H - cJ_0 m_{S2} + x \frac{J_0}{\sqrt{\alpha}} \sqrt{c(1-c)m_{S2}^2 + cP_{S2}(1-P_{S2})} \right) \right] (2.39)$$

where  $J_0 = \alpha J$ , similar to the previous sections.

Let us compare this result to the replica symmetric solution (2.29) in the previous

section. For big coordination numbers  $\alpha \approx z$  and we can see that the results look similar. The term  $P_{S2}(1-P_{S2})$  measures the spin fluctuations in sublattice  $S_2$ . The big problem is that these fluctuations include the spatial and the thermal fluctuations of the spin configuration. And there is no obvious way, how we could extract the Edward Anderson parameter from the expression under the square root. However by the comparison we can see that this solution contains all the necessary ingredients: the sublattice magnetizations and their fluctuations as well as an expression for the fluctuations of the vacancies c(1-c). Thus we have a good reason to assume, that the Bethe mean-field ansatz captures all the essential features of the system.

We will now focus on the limit of  $T \to 0$ , where we automatically get rid of the thermal fluctuations and get a solvable set of equations. Before we can do this we will have to find a way how we distinguish the different phases in the ground state.

#### 2.4.3 An order parameter for the DAFF ground state

In the DAFF ground state every site has a well defined spin value of +1 or -1 and it makes no sense to define a local magnetization  $m_i$ . Of course we can again calculate the sublattice magnetizations by averaging over the whole lattice. However the sublattice magnetizations are zero in the domain state as well as in the paramagnetic state. Without the local magnetizations one cannot calculate the Edwards Anderson parameter. So is there a way to distinguish between these two phases in the ground state?

In the antiferromagnetic state all the spins of one sublattice are up and all spins of the other sublattice are down. When the antiferromagnetic order starts to break, clusters of opposite antiferromagnetic order appear and the bonds at the borders of these clusters are violated. The domain state consists of inter-penetrating clusters of opposite antiferromagnetic order. A quantity that can be measured in the ground state is the size of these clusters. Intuitively it is clear that smaller clusters are more

susceptible to thermal fluctuations than bigger clusters. So let us try the following approach. As a measurement of the order of the system we take the size of the biggest antiferromagnetic cluster. Even when the pure antiferromagnetic order is broken, this cluster may still span the whole system and will therefore be relatively stable against thermal fluctuations as the system is heated to finite temperatures. To get rid of the direct dependence on the size of the system, the size of the giant cluster is divided by the total number of present sites. That way we measure the probability that an arbitrary site is in the giant antiferromagnetic cluster. It is clear that if the system size is taken to infinity, this probability will drop to zero as soon as the spanning cluster disappears. The investigation of the connected clusters of a system is the basic problem of percolation theory. Usually the spanning cluster of a system disappears in a second order transition (see for example [33]).

Of course it is not clear how this new order parameter is exactly connected to the thermal behavior of the system. However we will see in the next section that it is very useful to get information about the ground state and the results will help us to make connections to the finite temperature case.

## 2.4.4 A Bethe MFT for the DAFF ground state

The ansatz for the Bethe MFT for the DAFF ground state is basically the same as for the finite temperature case. The spin order is propagated upward in the Cayley tree. We consider how the spin state of a site s on level L+1 depends on the spins of the connected sites on the level L below. Of course now we do not have to use the Boltzmann distribution and it is convenient to make slightly different ansatz. There is also the possibility that a site is degenerated, so that we will consider the following probabilities:  $\tilde{P}$  is the probability, that a site is present and has spin up.  $\tilde{M}$  is the probability that a site is present and has spin down.  $\tilde{D}$  is the probability that a site is present and is degenerated. Obviously  $\tilde{P} + \tilde{M} + \tilde{D} = c$ , where c is again the site

concentration. Thus, the condition that a site on the lower level has to be present to influence s is already included in these probabilities. Denoting the number of up spins on level L by l and the number of down spins by k the energy contribution of s is  $E_{up} = (l-k)J - H$  or  $E_{down} = -((l-k)J - H)$ . The spin of s is up, if  $E_{up} < 0$  and down, if  $E_{up} > 0$ . If  $E_{up} = E_{down}$ , then the spin is degenerated. One can see that field values H, which are a multiple of J, play a special role. Only for H = hJ, where h is an integer, there is the possibility of degenerated nodes. For (h-1)J < H < hJ all these degenerated nodes have spin down, for hJ < H < (h+1)J they have spin up. The sites which are not degenerated at H = hJ have the same spin state in the whole range (h-1)J < H < (h+1)J. Thus, the spin configuration of the lattice does only change at these special values of H. Therefore we will first focus on them.

The spin of s will be up, if k - l - h < 0. The probability that s has spin up is the sum of the probabilities of all the configurations on level L, where the inequality above is fulfilled. The probability that s is present and has spin up therefore becomes

$$\tilde{P}_{L+1} = c \sum_{k=0}^{\alpha} \sum_{l=0}^{k+h} C(k,l) \tilde{M}_L^k \tilde{P}_L^l \tilde{D}_L^{\alpha-k-l},$$
(2.40)

where C(k,l) is the degeneracy of having a configuration of k down spins, l up spins and  $\alpha-k-l$  degenerated spins:

$$C(k,l) = \begin{cases} \frac{\alpha!}{k! l! (\alpha - k - l)!} & \text{if } \alpha - k - l > 0 \\ 0 & \text{else} \end{cases}$$
 (2.41)

From now on we will assume that the probabilities are independent of the level, so that we can drop the level index. The probability that s has spin down is

$$\tilde{M} = c \sum_{k=0}^{\alpha} \sum_{l=k+h+1}^{\alpha} C(k,l) \tilde{M}^k \tilde{P}^l \tilde{D}^{\alpha-k-l}$$
(2.42)

And the probability that s is degenerate is

$$\tilde{D} = 1 - c + c \sum_{k=0}^{\alpha} C(k, k+m) \tilde{M}^k \tilde{P}^{k+h} \tilde{D}^{\alpha-2k-h}$$
 (2.43)

Let us now consider the probabilities that a site which is present has certain spin state: P,M and D. We have  $\tilde{P}=cP$ ,  $\tilde{M}=cM$  and  $\tilde{D}=1-\tilde{M}-\tilde{P}=1-c(\tilde{M}+\tilde{P})=1-c+cD$ . For these probabilities we get the recursion formulas:

$$P = \sum_{k=0}^{\alpha} \sum_{l=0}^{k+h-1} C(k,l) (cM)^k (cP)^l (1-c+cD)^{\alpha-k-l},$$
 (2.44)

$$M = \sum_{k=0}^{\alpha} \sum_{l=k+h+1}^{\alpha} C(k,l) (cM)^k (cP)^l (1-c+cD)^{\alpha-k-l},$$
 (2.45)

$$D = \sum_{k=0}^{\alpha} C(k, k+h) (cM)^k (cP)^{k+h} (1-c+cD)^{\alpha-2k-h}$$
 (2.46)

One can easily check, that the validity condition M + P + D = 1 is fulfilled. We would have gotten these equations immediately if we had started by considering the bond diluted case. The bond concentration in the Bethe lattice is exactly the same as the site concentration c, because in the construction of the Bethe lattice one adds exactly one bond for every new site. Thus we can see that for the Bethe lattice site dilution and bond dilution are equivalent.

Physically relevant is the case of continuous H. We can get the probabilities for hJ < H < (h+1)J simply by adding D to P. This corresponds to recursion relations, where D=0 and the second sum in (2.44) goes go k+h instead of k+h-1. From now on I will focus on this case.

These equations can be solved by iteration. The solution for  $\alpha = 7$  and h = 2, that is 2J < H < 3J, is shown in figure 2.6. For a low site concentration the magnetic field is dominant and the magnetizations of both sublattices are the same. As soon as the concentration reaches a certain value, the iteration does not converge

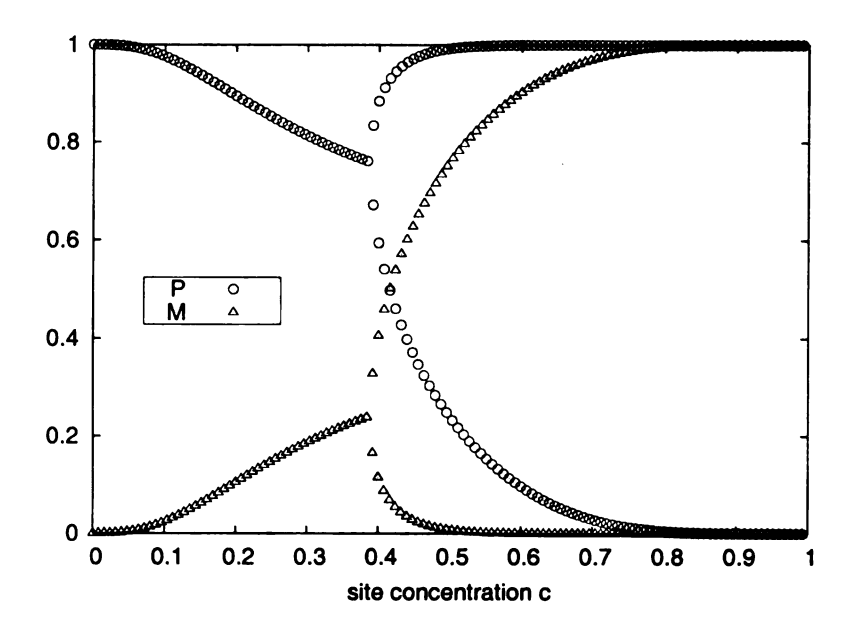


Figure 2.6: Solutions of the recursion relations for P and M for  $\alpha = 7$  and 2J < H < 3J.

against a single value any more, but oscillates between two values. This is the onset of antiferromagnetic order. The sublattice magnetizations become different. That is why the probabilities change between two values from level to level.

However this oscillating solution is problematic, because it must be unstable for the following reason. Since we propagate the order strictly upward, the sites on level L are completely independent of each other. That is why they cannot be organized as one sublattice. More likely we expect that both solutions for the probabilities come together on the same level. The natural way to take this fact into account is to average over the different sublattice probabilities during each iteration step. Thus, we have to make a different ansatz for the region, where the sublattice symmetry is broken. In order to do this it is convenient to consider slightly different probabilities.

Let us divide the Bethe lattice into sublattices S1 and S2; all even levels belong to S1, all odd levels to S2. There are two possible types of antiferromagnetic order: All spins of S1 are up and all spins of S2 are down and the other way round. Let

us denote the probability that a site s follows the first type by A and the probability that it follows the other type by B.

If s is on sublattice S1 then the recurrence relation for A is

$$A = \sum_{k=0}^{\alpha} \sum_{l=0}^{k+h} C(k,l) (cA)^k (cB)^l (1-c)^{\alpha-k-l}$$
 (2.47)

because on S1 A1 is favored by the field and hJ < H < (h+1)J. If s is on S2 then the field favors the opposite order, so that

$$A = \sum_{k=0}^{\alpha} \sum_{l=k+h+1}^{\alpha} C(k,l) (cB)^k (cA)^l (1-c)^{\alpha-k-l}$$
 (2.48)

Now we can easily average over these two different cases:

$$A = \frac{1}{2} \sum_{k=0}^{\alpha} \sum_{l=k+h+1}^{\alpha} C(k,l) (cA)^{k} (cB)^{l} (1-c)^{\alpha-k-l} + \frac{1}{2} \sum_{k=0}^{\alpha} \sum_{l=0}^{k+h} C(k,l) (cB)^{k} (cA)^{l} (1-c)^{\alpha-k-l}$$
(2.49)

B is then simply B = 1 - A. The solution for  $\alpha = 7$  and h = 2 is shown in figure 2.7.

The iteration now always converges against a single value. The solution for A and B are shown within the same plot. There is a big regime where both types of antiferromagnetic order are present with the same probability so that the staggered magnetization is zero. As soon as the concentration reaches a critical value long range order appears in a discontinuous jump. Which cluster disappears depends on the starting values of the iteration.

We can now use these probabilities to get a recursion formula for the order parameter for the DAFF ground state: the probability that a node is in the giant antiferromagnetic cluster (GAC). To do this it is useful to introduce some new no-

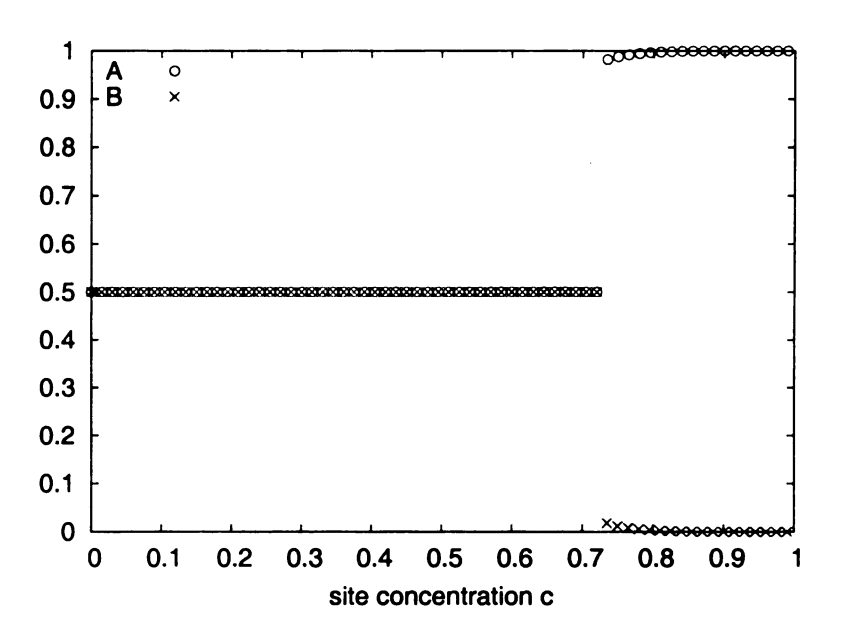


Figure 2.7: Solution for the recursion relations for A and B for  $\alpha = 7$  and 2J < H < 3J.

tations: The probability that a node is in the giant cluster with antiferromagnetic order corresponding to A is denoted by  $A_{\infty}$ . The probability that a nodes follows the order of type A but is not in the corresponding giant cluster is  $A_x = A - A_{\infty}$ . We define the analogous probabilities for the other order type B:  $B = B_x + B_{\infty}$ .

We can calculate  $A_x$  in the following way. The site s is not in the giant cluster, if all its connected neighbors on level L, which have follow order type A are also not in the giant cluster:

$$A_{x} = \frac{1}{2} \sum_{k=0}^{\alpha} \sum_{l=k+h+1}^{\alpha} C(k,l) (cA_{x})^{k} (cB)^{l} (1-c)^{\alpha-k-l}$$

$$+ \frac{1}{2} \sum_{k=0}^{\alpha} \sum_{l=0}^{k+h} C(k,l) (cB)^{k} (cA_{x})^{l} (1-c)^{\alpha-k-l}$$
(2.50)

Analogously,

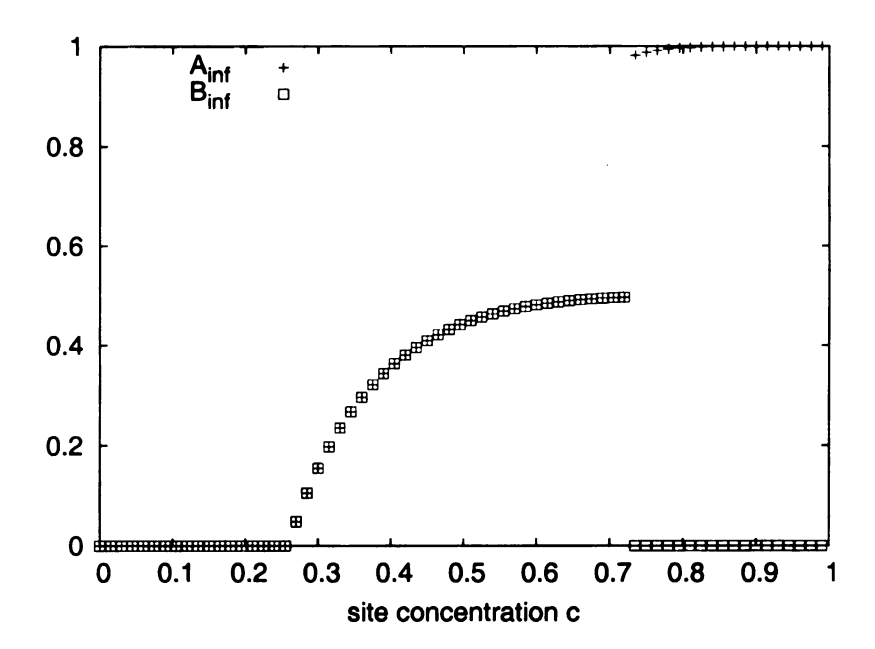


Figure 2.8: Solution of the recursion relations for  $A_{\infty}$  and  $B_{\infty}$  for  $\alpha = 7$  and 2J < H < 3J.

$$B_{x} = \frac{1}{2} \sum_{k=0}^{\alpha} \sum_{l=k+h+1}^{\alpha} C(k,l) (cB_{x})^{k} (cA)^{l} (1-c)^{\alpha-k-l} + \frac{1}{2} \sum_{k=0}^{\alpha} \sum_{l=0}^{k+h} C(k,l) (cA)^{k} (cB_{x})^{l} (1-c)^{\alpha-k-l}$$
(2.51)

From  $A_x$  and  $B_x$   $A_\infty$  and  $B_\infty$  are easy to calculate. The results are shown in figure 2.8.

One can clearly distinguish three different phases. For high concentrations the whole lattice is organized in antiferromagnetic long range-order. As the concentration decreases this order is suddenly broken and a cluster of opposite antiferromagnetic order appears. In this phase the whole lattice consists of two spanning antiferromagnetic clusters. As the concentration decreases further these two giant clusters disappear in a second order transition. All ordered clusters of the lattice have then only finite size.

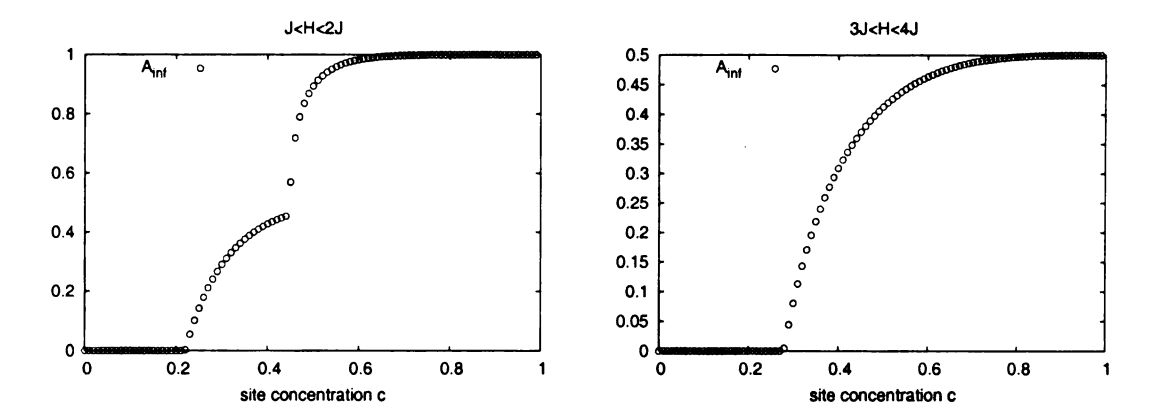


Figure 2.9: Solution of the recursion relations for  $A_{\infty}$  for  $\alpha = 7$  and J < H < 2J as well as 3J < H < 4J

The standard percolation threshold of the Bethe lattice is  $c = 1/\alpha = 0.14$ . We can see that the second transition lies above that value at c = 0.26. Thus, this transition is an combined effect of the loss of antiferromagnetic order and the loss of connectivity. At this transition the number of spins that have to be flipped to flip a whole cluster reduces from  $\mathcal{O}(N)$  to  $\mathcal{O}(1)$ . Thus it is reasonable to assume that this transition in the ground state corresponds to the transition from the domain state to the paramagnetic state at small finite temperatures.

Figure 2.9 shows the results for J < H < 2J and 3J < H < 4J. One can see that the transition from the one giant cluster to the two giant cluster state becomes smooth for h = 1. For h = 3 the state with just one giant cluster completely disappears.

However, for values of H that are close to zJ the model becomes pathological. For H > zJ all the spins are flipped into ferromagnetic order. Thus, we expect for big values of H also the existence of a ferromagnetic giant cluster. This feature is not captured by the presented model. Due to the average over both sublattices in equation (2.50) the loss of antiferromagnetic order as an effect of the emergence of ferromagnetic order is not predicted correctly.

This problem does not appear in the first ansatz (2.44), since the emergence of

ferromagnetic order can be described in terms of P and M. In the region where both sublattices are symmetric, this ansatz is working correctly. Thus, we have to combine these different approaches to get an accurate description of the full phase diagram.

The probability that a node is in the GAC  $P_{GAC}$  can also be calculated from M and P. We introduce similar notations as before:  $P_{\infty}$  is the probability that a site has spin up and is on the GAC.  $P_x$  is the probability that a site has spin up and is not on the GAC.  $M_{\infty}$  is the probability that a site has spin down and is on the GAC. Finally  $M_x$  is the probability that a site has spin down and is not on the GAC. Of course we have the relations  $P = P_x + P_{\infty}$  and  $M = M_x + M_{\infty}$ .  $P_{GAC}$  is obviously  $P_{GAC} = P_{\infty} + M_{\infty}$ .  $M_x$  and  $P_x$  can be calculated analogous to  $A_x$  and  $B_x$ :

$$P_x = \sum_{k=0}^{\alpha} \sum_{l=0}^{k+h} C(k,l) (cM_x)^k (cP)^l (1-c)^{\alpha-k-l}$$
 (2.52)

$$M_x = \sum_{k=0}^{\alpha} \sum_{l=k+h+1} C(k,l) (cM)^k (cP_x)^l (1-c)^{\alpha-k-l}$$
 (2.53)

The results for h=2 are shown in figure 2.10. One can see that  $P_{GAC}$  goes to zero at c=2.6, the same value that we have got from the other calculation. For bigger fields however the results deviate. At c=3.9 the sublattice symmetry is broken, as we have seen before.

We can now combine the different approaches to get a full and accurate picture of the phase diagram.  $A_{\infty}$  and  $B_{\infty}$  are appropriate order parameters to describe the antiferromagnetic phase and the transition to the domain state. For higher fields the solution with  $A_{\infty}$  and  $B_{\infty}$  becomes invalid in the domain state. P and M are appropriate order parameters to describe the first emergence of the GAC until the sublattice symmetry is broken. Between the symmetry breaking of the sublattices and the onset of antiferromagnetic order there is a region, where both approaches are not really accurate. This indicates that the behavior of the system in this region may

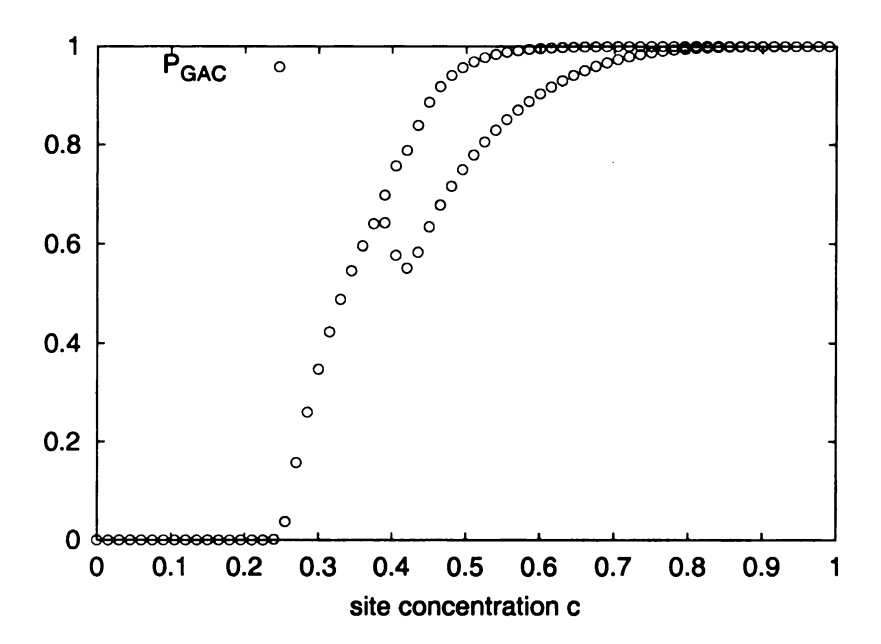


Figure 2.10: Solution of the recursion relations for  $P_{GAC}$  for  $\alpha = 7$  and 2J < H < 3J.

be more complex, than predicted from the  $A_{\infty}$  -  $B_{\infty}$  solution. The situation is similar as in the replica calculation, where one has to choose different order parameters for the spin glass phase.

Figure 2.11 shows the resulting phase diagram, which we get by solving the recurrence relations for all possible values of h and reading off the transition points. The phase boundary between the antiferromagnetic state and the domain state has been taken from the  $A_{\infty}$ - $B_{\infty}$  solution, the phase boundary between the paramagnetic state and the domain state from the P-M solution. The line that divides the domain state marks the onset of the symmetry breaking between the sublattices.

# 2.5 Conclusion

Let us summarize the results from the different mean-field calculations. The DAFF phase diagram exhibits three different phases: the antiferromagnetic phase, the para-

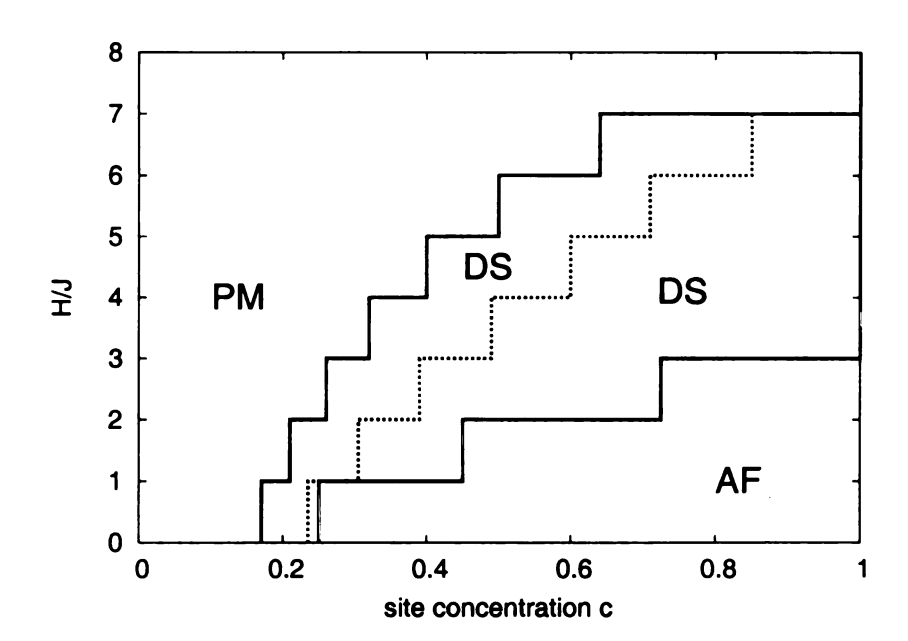


Figure 2.11: Phase diagram from the Bethe lattice MFT with  $\alpha=7$ . AF stands for the antiferromagnetic state with one giant cluster, DS for the domain state with two giant clusters, and PM for the paramagnetic state without any spanning clusters. The line which divides the domain state marks the onset of the symmetry breaking between the sublattices.

magnetic phase and an intermediate phase. In the intermediate phase the replica symmetry is broken, which is the classical feature of a spin glass phase. The local mean field calculations have shown that in this phase the lattice consists of domains of opposite antiferromagnetic order. We have argued that an appropriate order parameter to describe these phases in the ground state, is the probability that a node is in the giant antiferromagnetic cluster. On the Bethe lattice we have found that there is a phase with one giant cluster, a phase with two giant clusters and a phase with only finite-sized ordered clusters. These results shed a new light on the physical reasons for the DAFF phase transitions at low temperatures. Competing antiferromagnetic clusters percolate through the lattice. The infinite size of these clusters makes them stable against thermal fluctuations. As the infinite clusters disappear the system becomes paramagnetic. Both transitions can therefore be understood as percolation transitions. In the antiferromagnetic - domains state transition one cluster of opposite antiferromagnetic order percolates through the ordered lattice. In the second transition two spanning clusters disappear.

All the results of this section are based on mean-field assumptions, which are only valid in higher dimensions. In the next chapter I will present the results of exact ground state simulations in three dimensions, so that the accuracy of the mean-field results can be tested.

The mean-field technique on the Bethe lattice, which has been presented in the last section, offers many possibilities for further investigations. Using the ansatz of section 2.4.2 one could also try to investigate the giant clusters at finite temperatures. Furthermore the general method can also be applied to other systems. The big advantage over the replica method is that all necessary assumption can be based on physical considerations.

## Chapter 3

# Numerical simulations of the

# DAFF ground state

This chapter presents the numerical simulations of the DAFF ground state. The first section introduces the algorithm which has been the basis for the calculations. Section 3.2 presents a schematic study for the cubic and the BCC lattice which results in the phase diagrams for these lattices. In the last section 3.3 the exact ground state configurations are compared to the results of a local mean-field simulation.

# 3.1 An effective algorithm for the ground state calculation

The ground state calculation of the RFIM and the DAFF on a bipartite lattice can be mapped to the maximum flow problem, a classical combinatorial problem from computer science. Since there are effective algorithms that solve the maximum flow problem, this mapping gives us the possibility to calculate ground states in polynomial time. This was first introduced by Barahona in 1985 in [4], but similar mappings have already been used since the mid-seventies especially by the computer science

community. The mapping is based on the maximum flow - minimum cut theorem, one of the most important theorems for flow algorithms, which was found by Ford and Fulkerson [14]. A comprehensive review of mappings from a various number of disordered systems problems - including RFIM and DAFF - to flow problems is given in [3].

In this section I will review the mapping for the DAFF and RFIM, which is also the essential groundwork for the program, which I have used for my own numerical calculations. As a preparation I will start with a short introduction to the max flow problem and show the max flow - min cut theorem. Then I will demonstrate the mapping of the RFIM to maximum flow and describe the algorithm for the ground state calculation that follows from it. Finally I will present how a DAFF system can easily be mapped to a ferromagnetic system in a staggered field, so that the algorithm does also apply to the DAFF.

#### 3.1.1 Maximum flow and minimum cut

In the Maximum Flow problem we ask for the maximum flow through a network with limited bond capacity. A network is a directed Graph  $\mathcal{G}(V,A)$  with a set of nodes  $V = \{i \mid i = 1...N\}$  and a set of arcs  $A = \{(i,j) \mid i = 1...N, j = 1...N\}$ , where each arc has a capacity  $u_{ij} \geq 0$ . Each arc carries a flow  $x_{ij}$  from i to j, that has to satisfy the following constraint:

$$\forall (i,j) \epsilon A \quad 0 \le x_{ij} \le u_{ij}, \tag{3.1}$$

which just states that the flow may not exceed the capacity of the arc.

The flow springs from a distinguished node, the source s, and ends at another distinguished node, the sink t. No other nodes can inject or carry out flow. This is expressed in the following condition:

$$\sum_{\{j|(i,j)\in A\}} x_{ij} - \sum_{\{j|(j,i)\in A\}} x_{ji} = \begin{cases} f & if \ i = s \\ -f & if \ i = t \\ 0 & else \end{cases}$$
(3.2)

A flow that satisfies (3.2) is called *feasible*. The aim of the Maximum Flow problem is to find the maximum feasible flow f of a given network.

Obviously, even in a network with a maximum flow not all of the arcs have to carry their maximum possible flow. More likely there will be a "bottleneck", a narrow passage in the network, which determines the maximum flow. This intuitively clear fact is stated formally by the very useful min cut - max flow theorem.

Let us first clarify the terms. A *cut* is a partition of the node set V into two subsets S and  $T = V \setminus S$ , denoted by [S, T]. We are considering the case, where  $s \in S$  and  $t \in T$ , which is called s-t-cut. The capacity of a cut is defined as

$$u[S,T] = \sum_{(i,j)\in(S,T)} u_{ij},\tag{3.3}$$

where it is important to note, that sum goes only over the arcs, which go from S to T. A minimum cut is an s-t-cut, whose capacity is not bigger than those of all other s-t-cuts. Thus the minimum cut is the formal description of the bottleneck of the network. Of course the minimum cut does not have to be unique, there may be several partitions whose cut capacity has the same minimal value. The theorem of Ford and Fulkerson [14] is now easy to state and to prove.

**Theorem** The maximum flow of a given network is equal to the capacity of its minimum cut.

**proof** Let us consider a given feasible flow  $x_{ij}$  of total value f and an arbitrary s-t-cut [S, T]. Summing up the feasibility condition (3.2) for every node that is in S

we get the flow f, that springs from the source. On the other hand the flow of all arcs, whose head and tail are in S cancels out. So that we finally get

$$f = \sum_{i \in S} \left( \sum_{\{j | (i,j) \in A\}} x_{ij} - \sum_{\{j | (j,i) \in A\}} x_{ji} \right) = \sum_{(i,j) \in (S,T)} x_{ij} - \sum_{(j,i) \in (T,S)} x_{ji}.$$
(3.4)

Since  $0 \le x_{ij} \le u_{ij}$  it immediately follows that

$$f \le \sum_{(i,j)\in(S,T)} u_{ij} = u[S,T] \tag{3.5}$$

Since (3.5) holds for all possible cuts, the flow f has to be less or equal than the minimum cut. Thus every s-t-cut, whose capacity is fully used, has to be a minimum cut and the flow it carries is the maximum flow. On the other hand the flow from s to t can always be increased, if the flow is less than the minimum cut capacity, since all cuts have free capacity. Hence the maximum flow has to equal the minimum cut capacity.

An immediate conclusion of the max flow - min cut theorem is that we can find a minimum cut of a graph by finding its maximum flow. We only have to look for a set of arcs with maximal flow, which separates s from t. This can be done effectively by a breadth first search starting at s or t.

## 3.1.2 Mapping to maximum flow

Now we are ready to connect the maximum flow problem to the ground state calculation. We will start by minimizing a Hamiltonian of the form of the RFIM. Below we will see that for a bipartite lattice it is easy to bring the DAFF Hamiltonian into this form.

$$\mathcal{H} = -J \sum_{\langle ij \rangle} S_i S_j - \sum_i h_i S_i, \tag{3.6}$$

The first sum goes over all neighbors of the lattice and  $h_i$  is the magnetic field at site i.

Now it is useful to interpret the lattice of spins as a Graph  $\mathcal{G}(V, A)$ . Every spin is a site in the graph and every coupling between the neighbors i and j is represented by an arc  $(i, j) \in A$  with capacity J. This means of course that the arcs are symmetric. To include the magnetic field we add two new nodes s and t and connect them to all of the already existing nodes in the following way:

- If  $h_i > 0$  add an arc (s,i) with capacity  $h_i$ .
- If  $h_i < 0$  add an arc (i,t) with capacity  $|h_i|$ .

Fixing the spin of s up and the spin of t down we can write the Hamiltonian (3.6) as

$$H = -\sum_{(i,j)\in A} J_{ij} S_i S_j, \tag{3.7}$$

where A is the arc-set of the extended graph and  $J_{ij}$  is the capacity of arc (i, j). Now let S be the set of all sites with spin up and T the site set with all spins down. Then we can rewrite (3.6) as

$$H = \frac{1}{2} \left( -\sum_{(i,j)\in A} J_{ij} + 2 \sum_{(i,j)\in (S,T)} J_{ij} \right). \tag{3.8}$$

The first term would be the energy of the system, if all the bonds had been satisfied. For all the bonds, which are in fact not satisfied the second term adds the corresponding coupling energy, which the system has to pay for the violation. The two in this term takes into account, that we have already abstracted this energy in the first term. The second term is exactly twice the capacity of the cut [S,T] and obviously H is minimal if this term becomes minimal. Furthermore s has to be in S and t has to be in T since their spins are fixed. Thus the spin configuration of the ground state can be found by finding the minimum cut of the extended Graph. The

minimum cut separates the set of all up spins from the set of all down spins. All sites, which are in the same set as s have spin up and all in the the T set have spin down. As shown above the minimum cut can be found by calculating the maximum flow of the lattice. This is important, because there already exist efficient algorithms that solve the max flow problem.

The most efficient and most commonly used algorithm is the preflow-push algorithm, which was introduced by Goldberg and Tarjan [15]. It comes in variety of versions. The theoretical upper bound is  $\mathcal{O}(|V|^3)$ , but practically most of the algorithms do much better. A comprehensive overview over the existing flow algorithms is given in [2]. A more compact review already focused on the physics applications is given in [3]. Usually one can take advantage of a wide range of already existing implementations. A good tip is Goldberg's implementation of his own algorithm. The program, which I have used for the ground state calculation and which was written by Thomas Barthel uses the Flow algorithm from the LEDA library [22]. LEDA is very convenient, because it also offers a wide range of graph data type objects.

The following description in "pseudo code" summarizes how the ground state of a given lattice sample can be calculated.

```
Create the following graph:
{Add one site i for every spin}
Add one arc (i,j) with capacity J for every coupling J_ij
Add a source node s and a sink node t
For every h_i>0 connect s to i with capacity h_i
For every h_i<0 connect i to t with capacity |h_i|}
```

Calculate the maximum flow of the graph.

//Do a breadth first search for the nodes,

//which are in the same set as s:

```
Put s into a node queue L
While(L is not empty)
{ Take the first node n of L
set the spin of n up
for all arcs a of n
{ if (flow through a is not maximal)
add its target node to the List L }
}
```

Do the same breath first search starting at t and set the spin of all found nodes down.

All nodes, which have not been found by any of the breadth first searches, are degenerate.

The first breadth first search finds the minimum cut with the minimal number of up spins. Thus these spins have to be down in all possible ground states. The second search finds the minimum cut with the minimal number of down spins. For the spins that where not reached by the searches, there are ground states where they are up and ground states where they are down. Thus they are degenerate.

## 3.1.3 Transforming the bipartite DAFF into a ferromagnet

The algorithm can be applied to the DAFF by mapping it to ferromagnet in a staggered field. A necessary precondition for this mapping is that the lattice of the DAFF is bipartite and can be divided into sublattice S1 and sublattice S2 as described in the introduction. Let us now make the following transformation of the spin values:

$$S_{i} = \begin{cases} +S'_{i} & \text{if site } i \text{ is in } S1\\ -S'_{i} & \text{if site } i \text{ is in } S2 \end{cases}$$

$$(3.9)$$

The spins of sublattice S2 are flipped. The bipartite condition guarantees that spins of S2 are only coupled to spins of S1. Thus, it is easy to express the DAFF Hamiltonian in terms of the new spin values:

$$\mathcal{H} = \sum_{\langle ij \rangle} J\epsilon_i \epsilon_j S_i S_j - \sum_i H\epsilon_i S_i = -\sum_{\langle ij \rangle} J\epsilon_i \epsilon_j S_i' S_j' - \sum_i \epsilon_i h_i S_i$$
 (3.10)

where J > 0 and  $h_i$  is a newly introduced staggered field:

$$h_{i} = \begin{cases} H & \text{if } i \text{ is in } S1\\ -H & \text{if } i \text{ is in } S2 \end{cases}$$

$$(3.11)$$

The transformed Hamiltonian can now be minimized by the algorithm described above. Afterward the spins of sublattice S2 have to be flipped, so that they represent the original spins of the DAFF.

## 3.2 Results of the ground state simulation

The algorithm which has been presented in the last section enables us to calculate the spin configuration of a given lattice. In this section we will take advantage of this algorithm to measure the order parameters of the DAFF ground state for concrete lattice samples. This enables us to compare the results of the mean-field theory to simulation results which consider the concrete geometry of the lattice and do not depend on any approximations.

I start with a short introduction to the calculation process and example results

of the square lattice. I will then present schematic studies and establish the phase diagrams for the cubic lattice and the BCC lattice.

#### 3.2.1 Measurement of the order parameters

In the mean-field chapter we have seen that an efficient criterion to characterize the different phases of the DAFF ground state is the existence of giant ordered clusters. For a given spin configuration it is easy to find the size of the ordered clusters. Practically on a computer this can be done by a *breadth first* search.

The results of the mean-field theory predict that there is a state with one giant antiferromagnetic cluster, a state with two giant antiferromagnetic clusters, and a state where no ordered clusters span the whole system. Therefore I measure the size of the biggest antiferromagnetic cluster (GAC1) and the size of the second biggest cluster (GAC2). The results are then normalized by the total number of present sites, so that effectively we measure the probability that a present site is in the GAC1 or GAC2, respectively. To capture the onset of ferromagnetic order due to high magnetic fields I also measure the probability that a site is in the biggest ferromagnetic cluster (GFC). Furthermore I measure the sublattice magnetizations and the fraction of degenerate sites.

The simulation process is the following. For a given sample of the linear size L and the applied magnetic field H the site concentration c is varied by randomly taking out more and more of the magnetic sites. The order parameters are measured after each small step of c. This is done n times, so that the results can be averaged. The standard deviation is a measurement for the fluctuations of the order parameters in different samples.

Figure 3.1 shows the results for a square lattice with L=400 and H=1.0J. There is no sharp transition and no stable state with two giant clusters. This has been predicted by the Imry and Ma argument, which has been presented in the

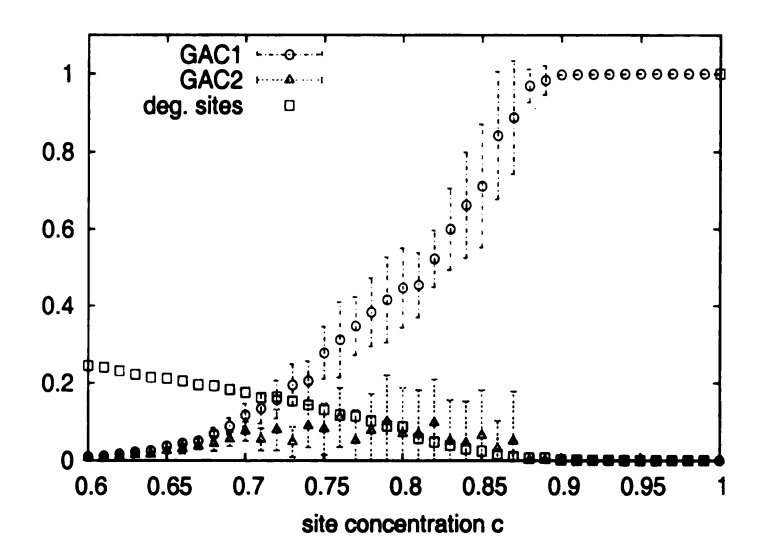


Figure 3.1: Square lattice with L=400 and H=1.0J averaged over 10 samples. The ordinate shows the probability that a site is in the biggest antiferromagnetic cluster (GAC1), the probability that a site is in the second biggest cluster (GAC2) and the fraction of degenerate sites (deg. sites).

introduction. Furthermore it follows from the Imry and Ma argument, that the small regime of perfect antiferromagnetic order at high concentrations c < 1 is unstable. It will vanish as the lattice size is increased to infinity. The square lattice is therefore a rather uninteresting case for the establishment of the phase diagram.

In three dimensions however the phase transitions should appear. In the following sections I present a detailed study of the transitions in the cubic and in the BCC lattice.

#### 3.2.2 The cubic lattice

Figure 3.2 shows the results for one sample of a cubic lattice of length L=70 and H=3.5J. The results looks very similar to the prediction of the mean-field theory. At c=0.813 the antiferromagnetic order is suddenly broken and a second giant cluster of opposite antiferromagnetic order appears. However, the second giant

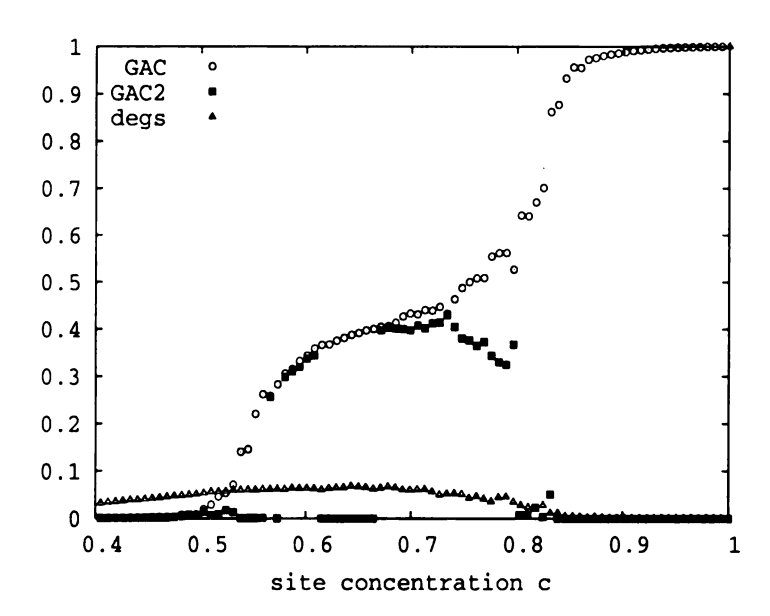


Figure 3.2: Cubic lattice with L=70 and H=3.5, one sample. The ordinate shows the probability that a site is in the biggest antiferromagnetic cluster (GAC), the probability that a site is in the second biggest cluster (GAC2) and the fraction of degenerate sites (degs).

cluster is not stable. In some regimes of the concentration it completely disappears. At  $c\approx 0.55$  the first giant cluster disappears in a second order transition. This leads to the following physical picture. At the first transition the half of the GAC flips to the opposite antiferromagnetic order. The flipping domains can all be connected and form a second giant cluster or they can be disconnected. The second transition is a percolation transition due to the further loss of antiferromagnetic order and connectivity. Even though H is not a multiple of J there is a small fraction of degenerate sites.

This general behavior does not depend on the size of the lattice as can be seen in figure 3.3. For smaller lattice sizes there are stronger fluctuations at the transition points. For bigger lattice sizes the transitions become sharper and it is easier to determine the transition point. As a compromise to the computation time the further studies focus on the cubic lattice with L=70. At this size the transition points can be

determined very accurately and the changes of the results as the lattice size is further increased are small. A cubic lattice with L=70 is already a good approximation for an infinite sized lattice.

The structure of the lattice in the different phases is illustrated in the 3d plots of figure 3.4. One can see that the clusters of opposite antiferromagnetic order become more interwoven as the concentration is decreased, which means that the ferromagnetic boundaries get bigger. The cluster boundaries display a pinning to the vacancy sites, to reduce the energy of violated antiferromagnetic bonds.

Figure 3.5 shows the results for L=70 and H=3.5J averaged over ten samples. The probability that a site is in the second GAC is strongly fluctuating, between 0 and 0.5. However, the lower end of the standard deviation is below zero, which indicates that the existence of the second cluster is a finite size effect and the second cluster will vanish in the limit of infinite lattices. The probability that a site is in the first GAC is only fluctuating at the phase transitions and in a small regime after the first transition. The domain state and the antiferromagnetic state are stable as well as the fraction of degenerate sites. Figure 3.5 also shows the staggered magnetization. As expected, the magnetization drops abruptly as the second giant cluster appears.

Figure 3.6 shows the results for L = 70 and H = 3J. Due to a rescaling procedure of the maximum-flow algorithm which has been used the value of integer values of the field cannot be realized exactly, but only with small deviations:  $H = (3 \pm 0.00002)J$  Still the fraction of degenerate spins is much higher than for H = 3.5. This is what we have expected from our discussion in section 2.4.4 in the mean-field chapter for integer values of the field.

The degenerate spins are not counted to any ordered cluster. They are influencing the second transition. If the degenerate spins are resolved by applying a very small staggered field then the transition point moves to slightly lower concentrations. However, it is reasonable not to resolve the degeneracy, because the degenerate spins do

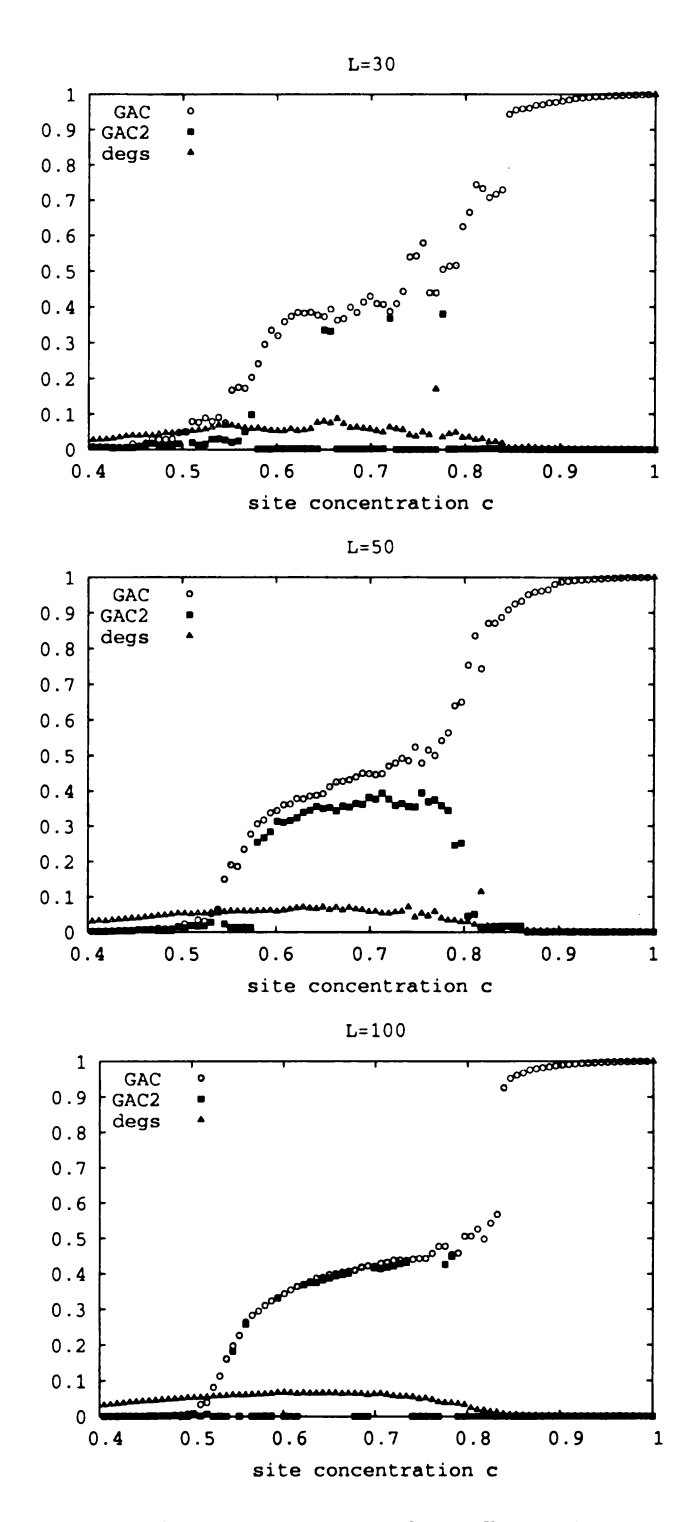


Figure 3.3: Single samples of the cubic lattice for different lattice sizes. The ordinate shows the probability that a site is in the biggest antiferromagnetic cluster (GAC), the probability that a site is in the second biggest cluster (GAC2) and the fraction of degenerate sites (degs).

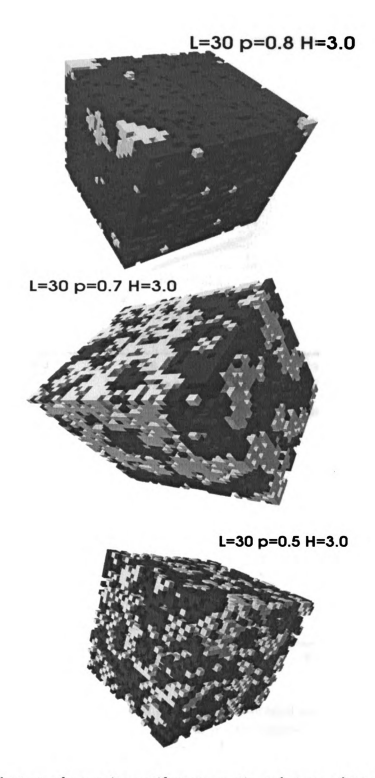


Figure 3.4: Clusters of opposite antiferromagnetic order are plotted in a different color. The first plot is a sample in the antiferromagnetic state close to the transition. The second plot shows a sample in the domain state. The last plot is a sample in the domain state close to the second transition.

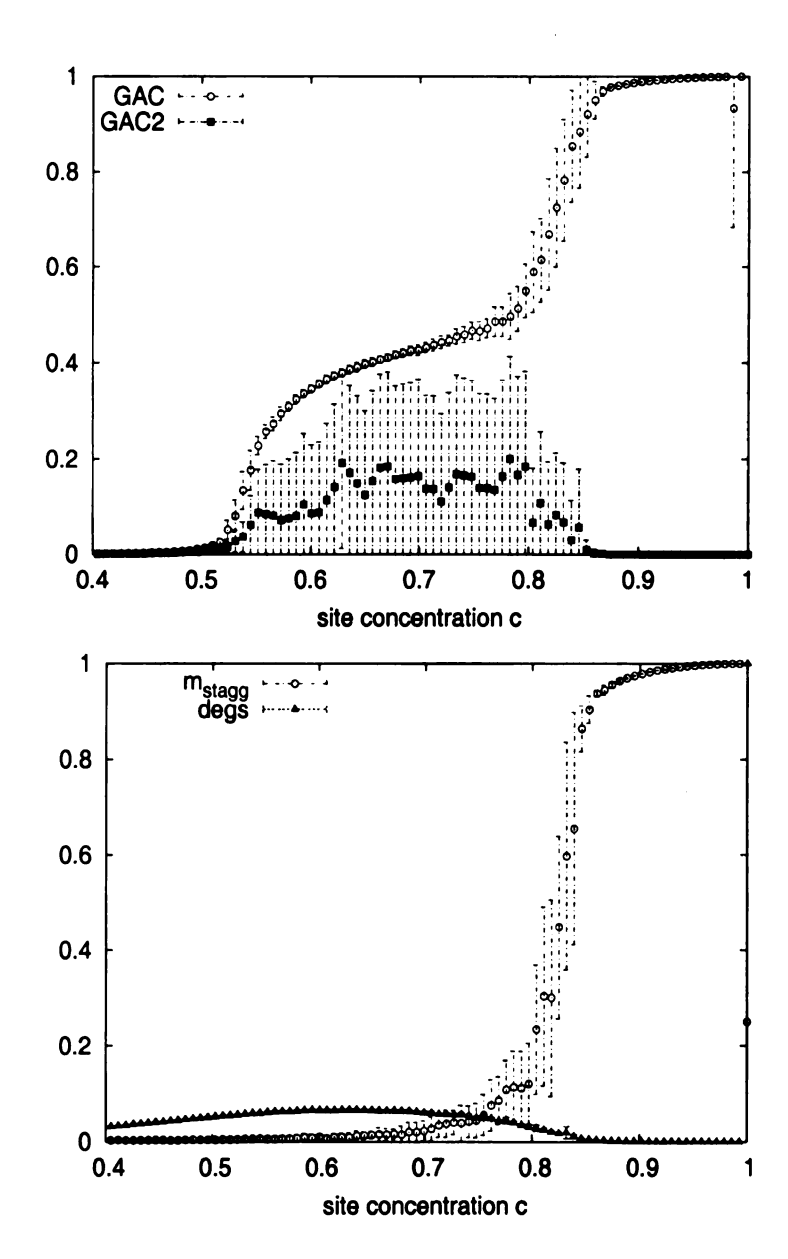


Figure 3.5: Cubic lattice with L=70 and H=3.5 averaged over 15 samples. The first plot shows the the probability that a site is in the biggest giant cluster (GAC) and the probability that it is in the second biggest cluster (GAC2). The second plot shows the staggered magnetization and the fraction of degenerate sites.

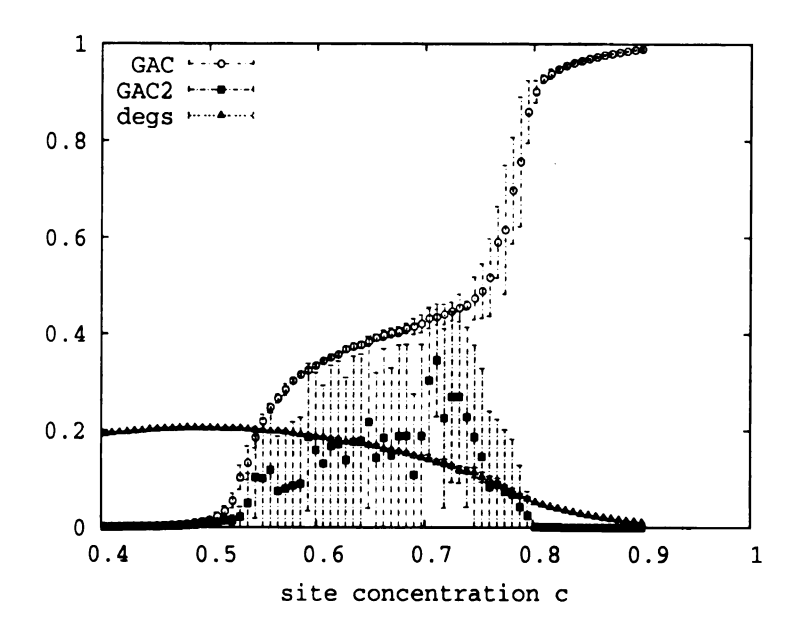


Figure 3.6: Cubic lattice with L=70 and H=3.0, averaged over ten samples. The ordinate shows the probability that a site is in the biggest antiferromagnetic cluster (GAC), the probability that a site is in the second biggest cluster (GAC2) and the fraction of degenerate sites (degs).

not stabilize the giant clusters. The fraction of degenerate spins is below the percolation threshold for the cubic lattice of c = 0.312, so that they cannot form a spanning cluster. Thus, the degenerate spins can only form finite clusters and the energy cost to flip one of these clusters is 0, so that they are not stable against thermal fluctuations.

The critical concentrations at which the transitions happen vary slightly from sample to sample. That is why the fluctuations are big at the transition points. Figure 3.7 demonstrates how one can estimate the transition points and their fluctuations from the data. For the second transition one has to cut off the tail, where the slope is starting to decrease again, because this is a finite size effect. A comprehensive introduction to the treatment of finite size effects in second order transitions can be found in [33].

Above H = 4.0J a giant ferromagnetic cluster (GFC) appears, as can be seen in figure 3.8. There may be sites at the borders of the ferromagnetic and antiferromagnetic antiferromagneti

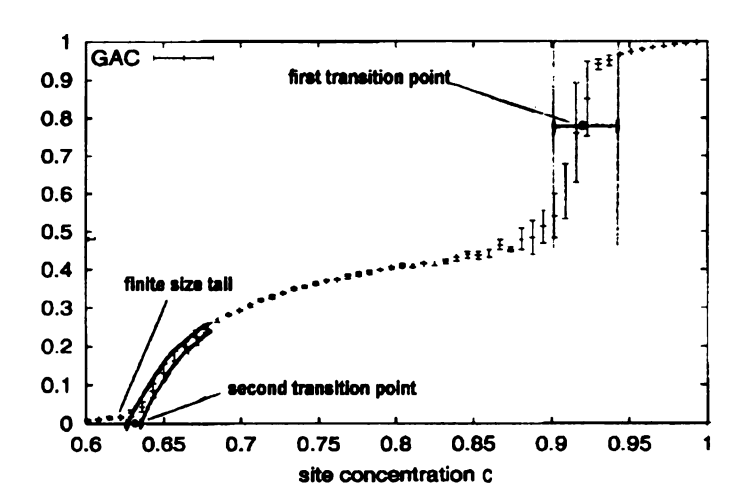


Figure 3.7: Demonstration how to estimate the critical points. Plot for a L=70 cubic lattice with H=4.5. The ordinate shows the probability that a site is in the biggest antiferromagnetic cluster (GAC).

netic clusters, which are counted to both clusters, so that the probabilities do not necessarily sum to one. The emergence of the giant ferromagnetic cluster happens close to the transition to the domain state. However, above H = 5.0 the GFC has a big finite size tail in the antiferromagnetic phase.

From a theoretical point of view it is natural to vary the dilution, since it corresponds directly to the disorder. However,in the real experiments it is of course more opportune to vary the magnetic field. Figure 3.9 shows that the different phases can of course also be seen for a varying field. Both methods lead to the same phase diagram.

The resulting phase diagram is shown in figure 3.10. The phase boundary between the paramagnetic phase and the domain state shows indeed the steps, which have been predicted by the Bethe lattice mean-field theory. At most of the steps the critical concentration even slightly decreases as the field is increased from integer values to slightly higher values. The phase boundary between the antiferromagnetic state and

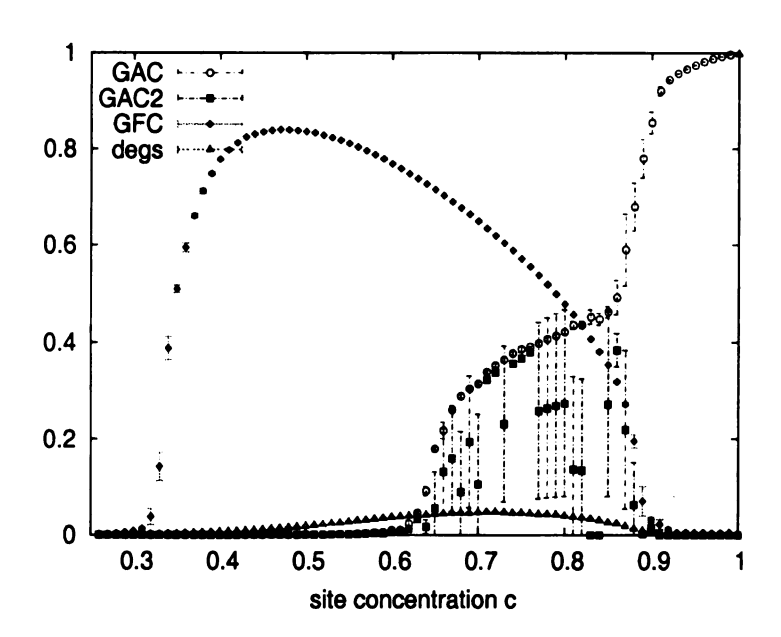


Figure 3.8: Cubic lattice with L=70 and H=4.1, averaged over three samples. The ordinate shows the probability that a site is in the biggest ferromagnetic cluster (GFC), the probability that a site is in the biggest antiferromagnetic cluster (GAC), and the probability that a site is in the second biggest antiferromagnetic cluster (GAC2), as well as the fraction of degenerate sites (degs).

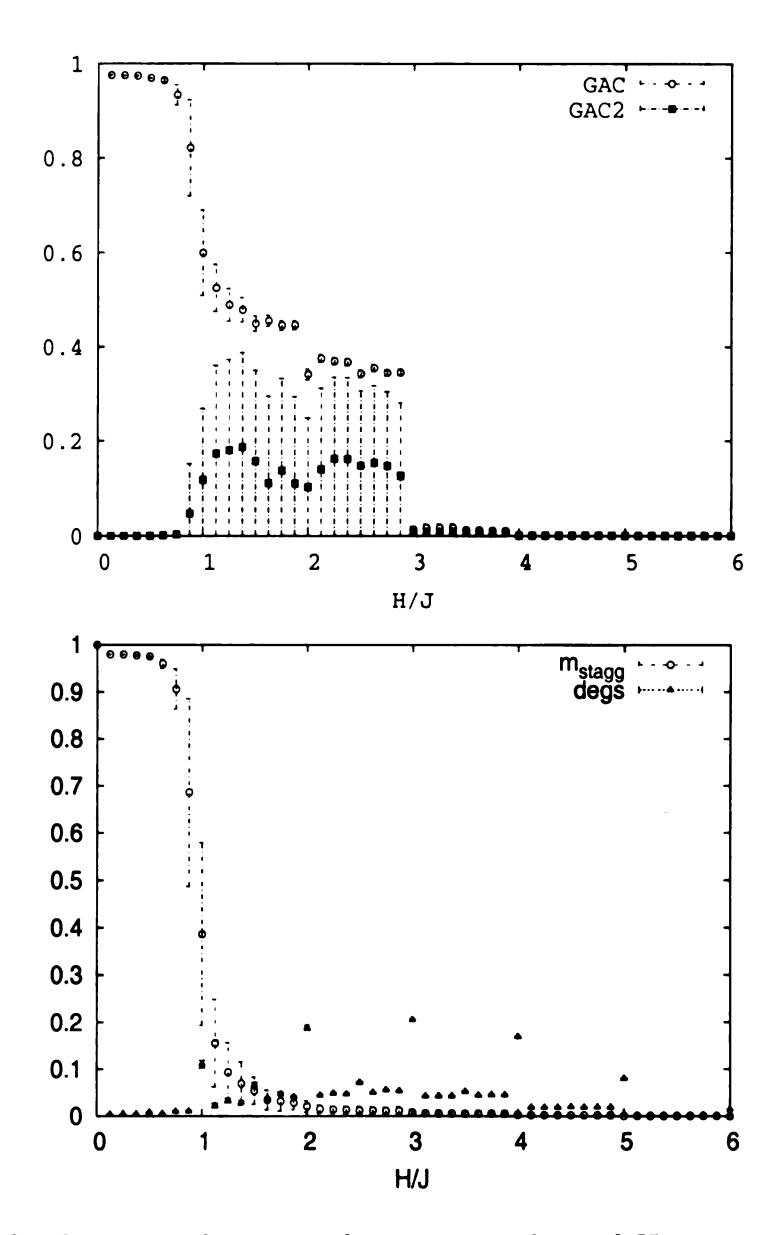


Figure 3.9: Cubic lattice with c=0.5 for varying values of H, averaged over fifteen samples. The first plot shows the probability that a site is in the biggest antiferromagnetic cluster (GAC) and the probability that a site is in the second biggest cluster (GAC2). The second plot shows the staggered magnetization and the fraction of degenerate sites. The results for the staggered magnetization are similar to those in [26].

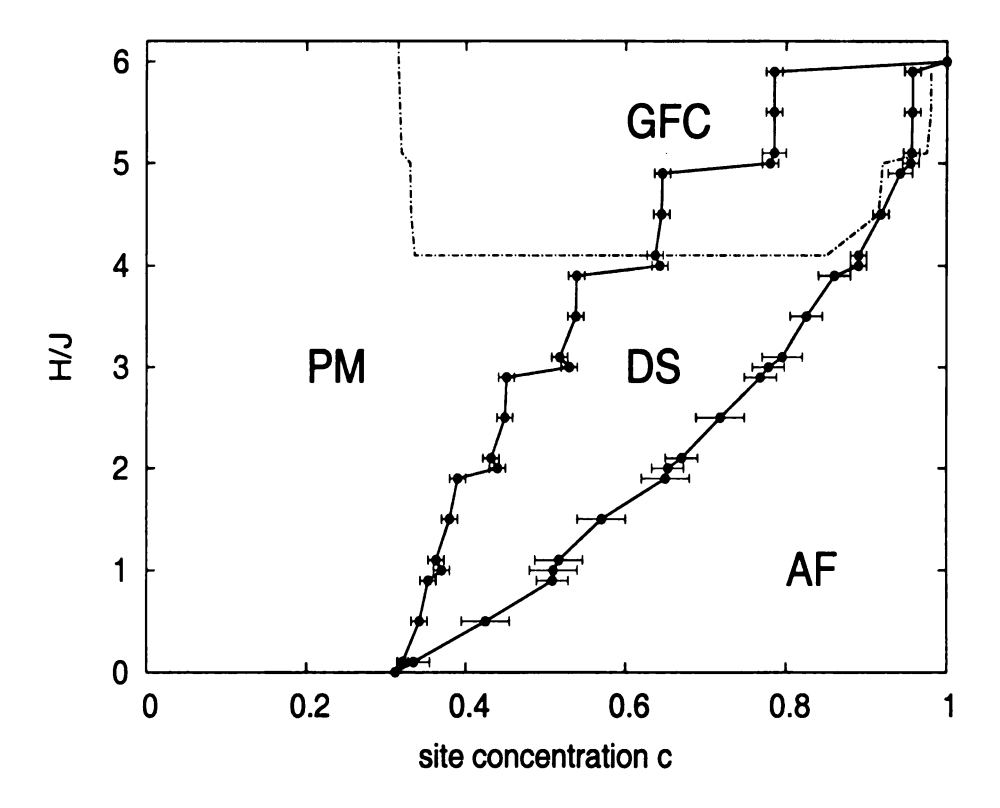


Figure 3.10: Phase diagram for the L=70 cubic lattice. AF stands for the antiferromagnetic phase, DS for the domain state, and PM for the paramagnetic state. The dotted line marks the region in which the giant ferromagnetic cluster (GFC) appears.

the domain state does not show a clear step structure.

The results for the cubic lattice show many agreements with the predictions from the mean-field theory. There are three phases, that can be categorized by the existence of giant clusters. However, we have found that for the cubic lattice the second giant cluster is highly unstable. The Bethe mean-field results which have been presented in section 2.4.4 were calculated for a coordination number z=8. But for the cubic case of z=6 it also predicts that the antiferromagnetic phase vanishes for fields bigger than H=3.0. The simulation results show, that this is not true in the real cubic lattice. The antiferromagnetic phase does not completely vanish as long as H<6.

#### 3.2.3 The BCC lattice

The BCC lattice corresponds to the crystal structure of  $Fe_cZn_{1-c}F_2$ . The structure of  $Fe_cZn_{1-c}F_2$  has been discussed in section 1.3. In addition to the dominant antiferromagnetic coupling there are also weak frustration bonds as well as weak ferromagnetic bonds. The frustration bonds violate the bipartite condition, which is necessary to apply the mapping to the maximum flow algorithm. But it is possible to include the ferromagnetic bonds, since ferromagnetic bonds within the same sublattice can be included in the graph construction for the algorithm. In the calculations for the BCC lattice I have therefore also included the ferromagnetic bonds. Their strength has been set exactly to the experimental value:  $J_F = -0.013J$ , where J is the strength of the dominant coupling. However, spot checks for different samples without this weak coupling did always lead to the same results.

Figure 3.11 shows the results for a L=50 BCC lattice with H=2.5. As for the cubic lattice the plot displays a transition from antiferromagnetic order to the domain state with two giant clusters and a transition to the paramagnetic state without any ordered clusters. The second giant cluster is again highly unstable. However, there is a region in the domain state from  $c\approx 0.58$  to  $c\approx 0.91$  where the fluctuations are very strong. These fluctuations did not display a dependence on the size of the BCC lattice, which indicates that the domain state is not stable in this regime.

A way to check the stability of a regime is to impose boundary conditions on the system and to see if this influences the results. Figure 3.12 shows the results for H=1.5 with and without antiferromagnetic boundary conditions within the same plot. The boundary conditions are applied to two opposite surface areas of the cube in such a way that they allow a perfect antiferromagnetic arrangement. All spins at these two surface planes are fixed in antiferromagnetic order. One can see that exactly in the regime with the big fluctuations the boundary conditions change the results. The abrupt transition is destroyed and the antiferromagnetic regime becomes

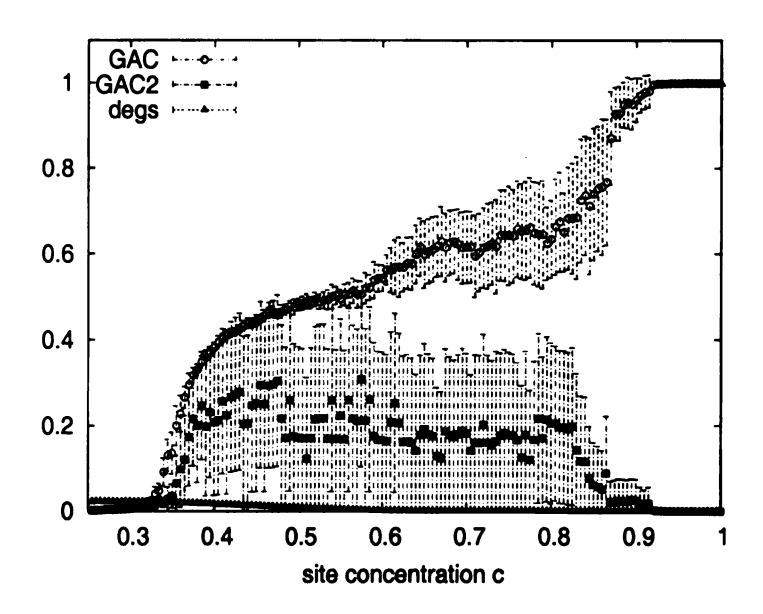


Figure 3.11: BCC lattice with L = 50 and H = 2.5, averaged over ten samples. The ordinate shows the probability that a site is in the biggest antiferromagnetic cluster (GAC), the probability that a site is in the second biggest cluster (GAC2) and the fraction of degenerate sites (degs).

bigger.

This boundary dependence happens in the whole range of the magnetic field. Antiferromagnetic boundary conditions have also been checked for the cubic lattice, which did not display this strong dependence. One reason for this is possibly that for the same number of total sites the number of surface sites in the BCC lattice is twice as big as the number of surface sites in the cubic lattice. The concentration regime in which the domain state is unstable can be seen best from the fluctuations of the sublattice magnetizations, as plotted in figure 3.13 for H=1.5. For the sublattice magnetizations there is no second transition so that the fluctuations nearly completely vanish. For the construction of the phase diagram I have used the sublattice magnetization data to get the phase boundary where the domain state becomes unstable, as demonstrated in figure 3.13. The error is estimated from the size of the small regime where the fluctuations already become noticeably small but do not yet

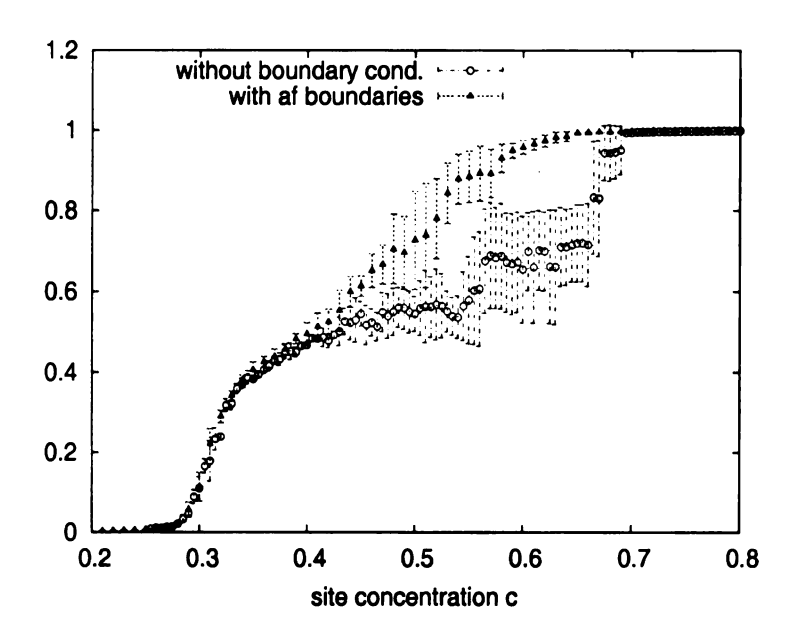


Figure 3.12: The probability that a node is in the GAC for a BCC lattice with L=50 and H=1.5 under different boundary conditions. Averaged over five samples.

vanish.

Figure 3.14 shows the results for a lattice with ferromagnetic boundary conditions and H=1.5. The antiferromagnetic phase is completely destroyed in favor of a domain state with big fluctuations. This indicates that the whole antiferromagnetic phase is also metastable. From the fluctuations of the sublattice magnetization one can see that the concentration value at which the domain state becomes stable does not change. Figure 3.15 shows that even at very small magnetic fields there is no antiferromagnetic state under ferromagnetic boundary conditions.

As for the cubic lattice a giant ferromagnetic cluster appears above H=4.0. All these results are summarized in the phase diagram in figure 3.16. The emergence of the GFC coincides with the onset of stability in the domain state. The phase boundary between the antiferromagnetic state and the domain state displays again the step structure, which we have first encountered in the mean-field solution. However, it is not as distinct as in the cubic case and the fraction of degenerate sites in the BCC

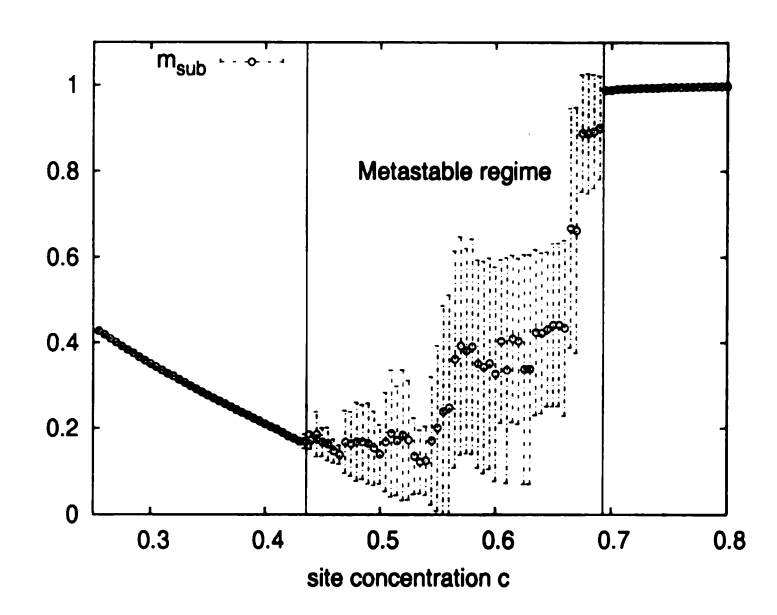


Figure 3.13: The sublattice magnetization averaged over both sublattices for a BCC lattice with L=50 and H=2.5, averaged over five samples.

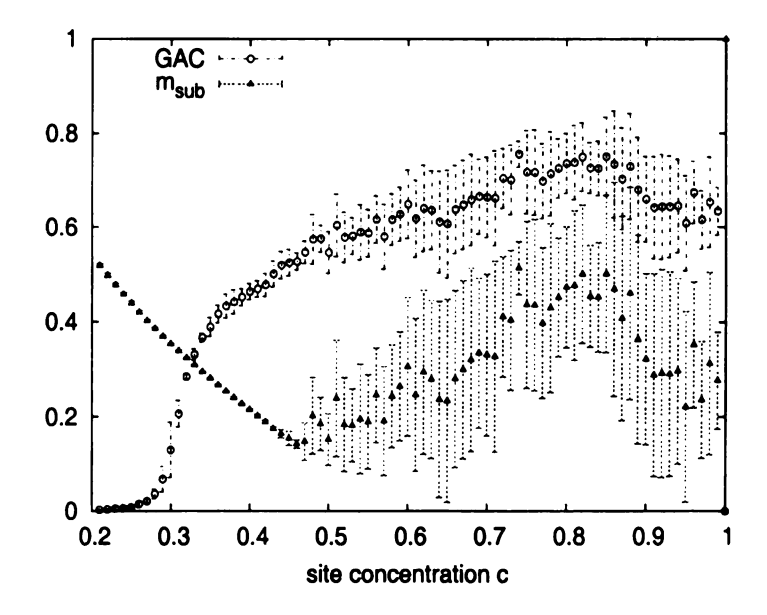


Figure 3.14: BCC lattice with L=50 and H=1.5 under ferromagnetic boundary conditions, averaged over five samples. The ordinate shows the probability that a site is in the biggest antiferromagnetic cluster (GAC), as well as the sublattice magnetization  $m_{sub}$ .

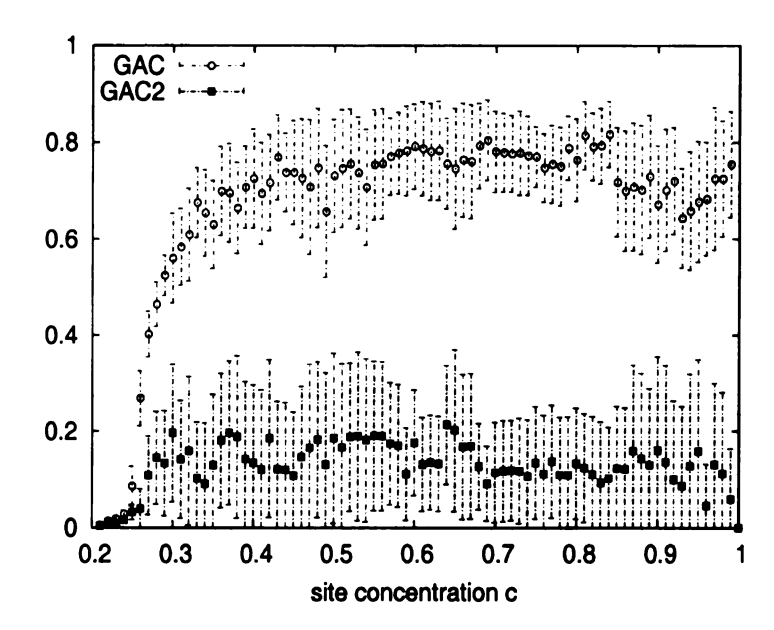


Figure 3.15: BCC lattice with L=50 and H=0.1 under ferromagnetic boundary conditions, averaged over five samples. The ordinate shows the probability that a site is in the biggest antiferromagnetic cluster (GAC) and the probability that a site is in the second biggest cluster (GAC2).

lattice is lower. The metastable antiferromagnetic phase vanishes above H=3.0 as has been predicted by the mean-field theory in section 2.4.4 for z=8 which corresponds to the coordination number of the Bethe lattice. It is reasonable that the line in the Bethe lattice solution at which the sublattice symmetry is breaking corresponds to the onset of metastability in the BCC lattice. Comparing the phase diagram for the BCC lattice with the phase diagram for the Bethe lattice (Figure 2.11) one can see the big similarity: The mean-field theory works already very well for the BCC lattice.

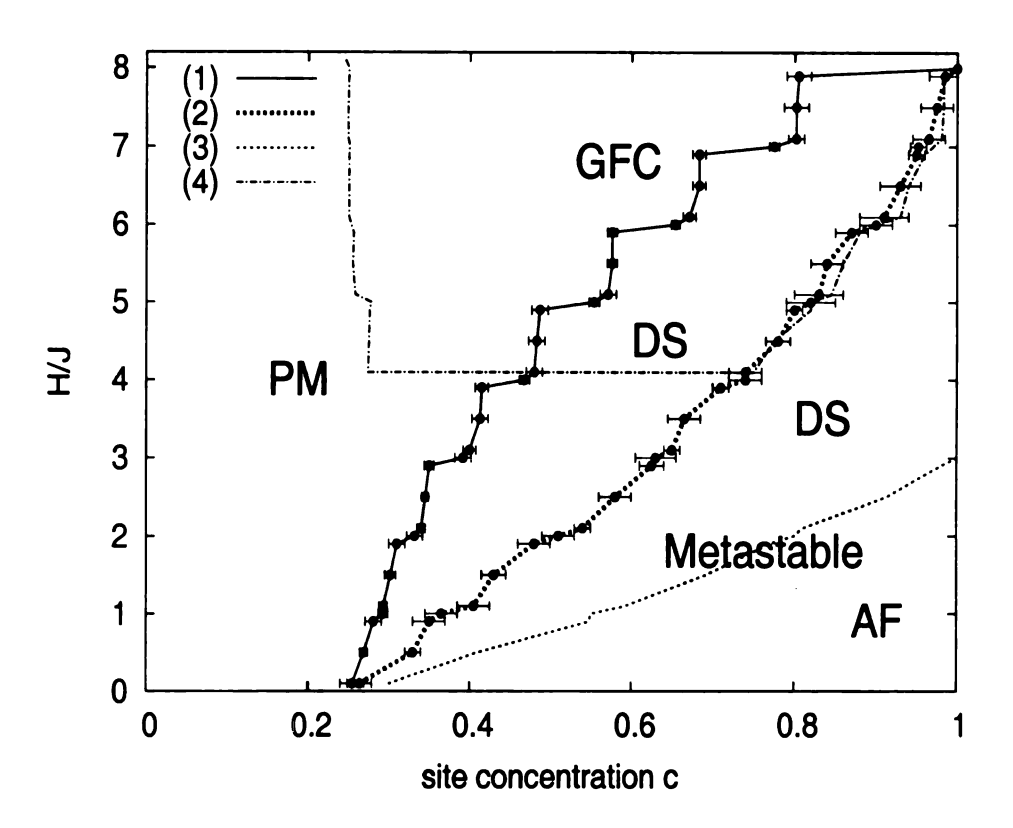


Figure 3.16: Phase diagram for the L=50 BCC lattice. Line (1) is the phase boundary between the paramagnetic state (PM) and the stable domain state (DS). Line (2) marks the onset of metastability in the domain state. Line (3) is the phase boundary between the metastable antiferromagnetic phase (AF) and the metastable domain phase. Line (4) marks the emergence of the giant ferromagnetic cluster (GFC).

# 3.3 Direct comparison of the LMF results to the DAFF ground state

The results from the ground state simulation are consistent with the results of the local-mean field simulations, which have been presented in section 2.3.2. The local mean-field calculations have also predicted three different phases and a region of metastability. In order to check how closely the deep temperature result of a local-mean-field simulation corresponds to the real ground state, I have also conducted a local mean-field study of the BCC lattice.

By doing a local mean-field simulation and an exact ground state calculation for the same specific lattice sample the results can be compared directly. A positive local magnetization is taken as spin up and a negative local magnetization as spin down. That way the fraction of sites which have the same spin value in the ground state and in the local mean-field result can be measured. The local mean-field procedure has been described in section 2.3.2. The simulations have been conducted with the following parameters: the convergence criterion  $\epsilon = 10^{-14}$ , the temperature steps during cooling  $\Delta T = 2 \cdot 10^{-4}$ , the start temperature T = 5 and the final temperature T=0.01. Because of the long computation times of the cooling procedure the linear size of the BCC lattice has been restricted to L=20. The comparison has been done for a field of H=2.5 and four different values of the concentration, so that all different phases are covered: the antiferromagnetic state, the metastable domain state, the stable domain state and paramagnetic state. Both different cooling procedures have been tested. Each concentration value has been simulated for ten different lattice samples. The results for the average fraction of equal sites and the corresponding standard deviation are shown in table 3.1.

The fraction of equal sites depends on the phase and the cooling procedure. All the samples for c = 0.95 have led to long-range order in zero-field cooling as well as

cooling	state	site concentration	fraction of equal sites	
zero-field	AF	0.95	0.54	$\pm 0.49$
	DS (metastable)	0.70	0.54	$\pm 0.11$
	DS (stable)	0.50	0.60	$\pm 0.06$
	PM	0.25	0.88	$\pm 0.01$
field	AF	0.95	0.43	$\pm 0.49$
	DS (metastable)	0.70	0.70	$\pm 0.15$
	DS (stable)	0.50	0.89	$\pm 0.02$
	PM	0.25	0.92	$\pm 0.05$

Table 3.1: Comparison of the local mean-field theory results to the real ground state. The calculations have been done for a L=20 BCC lattice with H=2.5.

in field cooling. However, about the half of the samples arranged themselves in the opposite type of antiferromagnetic order than the real ground state. Therefore the fraction of equal sites was either very close to one or very close to zero, which explains the big standard deviation of these values.

For the unstable domain state the zero-field cooling led to results where about half of the spins were equal to the ground state. This is not more than a pure random procedure would produce. In the case of field cooling a fraction of equal sites of 0.7 indicates that there is a slight tendency that the local magnetizations correspond to the ground state.

In the stable domain state the field cooling procedure leads to local magnetization patterns which are nearly the same as the ground state, whereas the result of zero-field cooling shows no strong correspondence. In the paramagnetic state both cooling procedures lead to local magnetizations, which correspond strongly to the ground state.

These results support the generally accepted assumption that the ground state of the DAFF determines the low temperature regime. The field cooling procedure leads to nearly the same results. Deviations in the metastable domain phase are a further indication of the metastability.

## Chapter 4

## Conclusion

We have established the phase diagrams for the DAFF ground state in the mean-field limit, for the BCC lattice and for the cubic lattice. We have found that the DAFF exhibits three different equilibrium phases: the antiferromagnetic state, the domain state and the paramagnetic phase. We have argued that the criterion for the domain state in the ground state is the existence of two out of phase antiferromagnetic clusters, which span the whole lattice. At low temperatures these clusters are stable against thermal fluctuations, because the total number of sites, which have to flipped to flip the whole cluster is of the order of the total number of lattice sites. The domain state should therefore display a glassy behavior without long range antiferromagnetic order. The prediction of these three phases for the low temperature regime are in agreement with the results of mean-field studies at finite temperatures [36], [29], [10]. However, one has to be aware that these approaches also ignore the thermal fluctuations.

Inferences for the RFIM. The criterion for the domain state can now also be applied to the RFIM. Seppälä et al. [30] study the 3d RFIM ground state by percolation methods. They start with a ferromagnetic ordered lattice and then increase the variations of the random field, so that spins start to flip to the opposite direction. They investigate the point where the flipped spins percolate through the lattice

and form a giant cluster. They interpret this percolation point as the transition to the paramagnetic state. However, it is clear that after the percolation threshold the lattice is spanned by two giant ferromagnetic clusters. As we have seen this does not correspond to the paramagnetic state but to the domain state. In the limit of very strong fluctuations of the random field all spins will align themselves with the local random field, so that the spin state will be a random configuration with half of the spins up and half of the spins down. The percolation threshold in three dimensions is c = 0.312 for the cubic lattice and c = 0.246 for the BCC lattice, where c is the site concentration. Therefore a random spin configuration with half of the spins up and half of the spins down will still form two interpenetrating spanning clusters in three dimensions. Hence there is no second transition for the RFIM, the ground state exhibits only the ferromagnetic state and the domain state. This is in agreement with the replica calculation of Mézard et al. [23]. A way to actually check the stability of the giant clusters against thermal fluctuations at low temperatures is possibly a Monte Carlo simulation starting with the exact ground state configuration.

These results reveal an important difference between the DAFF and the RFIM in the deep temperature regime. However, the additional phase of the DAFF gives no reason to claim that the transition between the long-range-ordered state and the domain state in the DAFF and the RFIM should not be in the same universality class. The jump-like appearance of this transition in the DAFF for the mean-field solution as well as for the 3d simulations in higher fields indicates that this transition is first order. For lower fields the transition seemed smoother so that there may be a tricritical point at which the transition changes from first order to second order. A tricritical point has been predicted for the RFIM within mean-field theory by Aharony in [1].

Results for the DAFF. For the BCC lattice and the mean-field limit we have found indications of metastability within the domain state. In the BCC lattice the actual state in a part of the domain phase and in the whole antiferromagnetic phase displays a strong dependence on the boundary conditions. It is an open question, why this effect does not appear in the cubic lattice. It is also an open question why the second giant cluster in the domain state is highly unstable.

A schematic experimental study of  $Fe_cZn_{1-c}F_2$  in the whole range of concentration would be very desirable. Important questions are if the antiferromagnetic phase does exist in the real systems and how the different phases can be distinguished. It would be very interesting to see if a phase diagram based on experimental data does also exhibit the step structure of the domain state - paramagnetic state phase boundary (see figure 3.16). Possibly this could even be the characteristic feature which helps to identify this phase boundary correctly.

As has been demonstrated by local-mean-field simulations [28] the weak frustration bonds which are present in  $Fe_cZn_{1-c}F_2$  play an important role for zero field cooling below a concentration of c = 0.63. It would be interesting to see how they influence the phase diagram presented here. A complete theoretical description of  $Fe_cZn_{1-c}F_2$  has to consider these bonds. This is an important possible extension of this work.

## Bibliography

- [1] A. Aharony. Tricritical points in systems with random fields. *Physical Review B*, 18(7):3318-3327, 1978.
- [2] R.K. Ahuja, T.L. Magnanti, and J.B. Orlin. Network Flows. Prentice-Hall, 1993.
- [3] M.J. Alava, P.M. Duxbury, C.F. Moukarzel, and H. Rieger. Exact Combinatorial Algorithms: Ground States of Disordered Systems. In C. Domb and J.L. Lebowitz, editors, *Phase Transistions and Critical Phenomena*, vol. 18. Academic Press, 2001.
- [4] F. Barahona. Finding ground states in random-field Ising ferromagnets. *Journal of Physics A*, 18:673–675, 1985.
- [5] D. P. Belanger. Experiments on the Random Field Ising Model. In A.P. Young, editor, *Spin Glasses and Random Fields*, pages 251–275. World Scientific, 1997.
- [6] A.J Bray and M.A. Moore. Scaling theory of the random-field Ising model. Journal of Physics C, 18:L927-L933, 1984.
- [7] J. Bricmont and A. Kupiainen. Lower Critical Dimension of the Random-Field Ising model. *Physical Review Letters*, 59:1829–1832, 1987.
- [8] R. Bruinsma. Random-field Ising model on a Bethe lattice. *Physical Review B*, 30(1):289–299, 1984.
- [9] J. L. Cardy. Random-field effects in site-disordered Ising anfiferromagnets. *Physical Review B*, 29(1):505–507, 1984.
- [10] J.R.L. de Almeida and R. Bruinsma. Replica symmetry breaking in random-field systems. *Physical Review B*, 35(13):7267-7270, 1987.
- [11] J.R.L. de Almeida and D.J. Thouless. Stability of the Sherrington-Kirkpatrick solution of a spin glass model. *Journal of Physics A*, 11(5):983-990, 1978.
- [12] S.F. Edwards and P.W. Anderson. Theory of Spin Glasses. *Journal of Physics* F, 5:965-974, 1975.
- [13] J. Esser, U. Nowak, and K.D. Usadel. Exact ground-state properties of disordered Ising systems. *Physical Review B*, 55(9):5866-5872, 1997.

- [14] L.R. Ford and D.R. Fulkerson. *Flows in Networks*. Princeton University Press, 1962.
- [15] A.V. Goldberg and R.E. Tarjan. A new approach to the Maximum-Flow problem. Journal of the ACM, 35:921-940, 1988.
- [16] G.S. Grest, C.M. Soukoulis, and K. Levin. Irreversibility and metastability in spin-glasses. I. Ising model. *Physical Review B*, 28(3):1495-1509, 1983.
- [17] A.K. Hartmann and U. Nowak. Universality in the three dimensional random-field ground states. *The European Physical Journal B*, 7:105-109, 1999.
- [18] M.T. Hutchings, B. D. Rainford, and H.J. Guggenheim. Spin waves in antiferromagnetic  $FeF_2$ . Journal of Physics C, 3:307-322, 1970.
- [19] J. Z. Imbrie. Lower Critical Dimension of the Random-Field Ising Model. *Physical Review Letters*, 53:1747–1750, 1984.
- [20] Y. Imry and S.-K. Ma. Random-Field Instability of the Ordered State of Continuous Symmetry. *Physical Review Letters*, 35:1399-1401, 1975.
- [21] A. R. King, V. Jaccarino, T. Sakakibara, M. Motokawa, and M. Date. Field induced "Exchange flips" in Randomly Diluted Antiferromagnet. *Physical Review Letters*, 47:117-120, 1981.
- [22] K. Mehlhorn and Stefan Naeher et al. LEDA, the library of efficient data types and algorithms.
- [23] M. Mézard and R. Monasson. Glassy transition in the three-dimensional random-field Ising model. *Physical Review B*, 50(10):7199-7202, 1994.
- [24] M. Mezard, G. Parisi, and A. Virasoro. *Spin Glass Theory and beyond*. World Scientific, 1987.
- [25] A.A. Middleton and D.S. Fisher. Three dimensional random-field magnet: Interface, scaling and the nature of states. *Physical Review B*, 65:134411, 2002.
- [26] E. Mueller-Hartmann and J. Zittarz. New Type of Phase Transition. *Physical Review Letters*, 33(15):893–897, 1974.
- [27] G. Parisi and N. Sourlas. Random Magnetic Fields, Supersymmetry, and Negative Dimensions. *Physical Review Letters*, 43:744-745, 1979.
- [28] E.P. Raposo and M.D. Coutinho-Filho. Local-mean-field numerical studies in  $Fe_xZn_{1-x}F_2$ . Physical Review B, 57(6):3495-3511, 1998.
- [29] C. Ro, G.S. Grest, C.M. Soukoulis, and K. Levin. Irreversibility in random-field ferromagnets and diluted antiferromagnets. *Physical Review B*, 31(3):1682–1685, 1985.

- [30] E.T. Seppälä, A.M. Pulkkinen, and M.J. Alava. Percolation in three-dimensional random field Ising magnets. *Physical Review B*, 66:144403, 2002.
- [31] D. Sherrington and S. Kirkpatrick. Solvable Model of a Spin Glass. *Physical Review Letters*, 35(26):1792–1796, 1975.
- [32] H.E. Stanley. Introduction to Phase Transitions and Critical Phenomena. Oxford Science Publications, 1971.
- [33] Dietrich Stauffer and Amnon Aharony. Introduction to Percolation Theory. Taylor & Francis, 1992.
- [34] J. von Boehm and P. Bak. Devil's Stairs and the Commensurate-Commensurate Transitions in CeSb. Physical Review Letters, 42:122–125, 1979.
- [35] K.G. Wilson. Renormalization Group and Critical Phenomena. 2. Phase Space Cell Analysis of Critical Behavior. *Physical Review B*, 4:3184–3205, 1971.
- [36] H. Yoshizawa and D.P. Belanger. Mean-field simulation of field-induced domains and hysteretic behavior in dilute Ising antiferromagnets. *Physical Review B*, 30(9):5220–5227, 1984.

